Transport properties of fluorinated surfactants: viscosity and diffusion of mixtures involving fluorinated alcohols

João de Oliveira Mateus Afonso

Thesis to obtain the Master of Science Degree in

Chemical Engineering

Supervisors:

Prof. Doctor Eduardo Jorge Morilla Filipe

Prof. Doctor Clare McCabe

Examination Commitee

Chairperson: Prof. Doctor Sebastião Manuel Tavares Silva Alves

Supervisor: Prof. Doctor Eduardo Jorge Morilla Filipe

Member of the Commitee: Prof. Doctor Luís Filipe Guerreiro Martins

November 2018

Acknowledgements

This project would not be possible without the support of several people to which I am very grateful.

First of all, I would like to demonstrate my deep gratitude to Prof. Eduardo Filipe, not only for the providing me with this amazing opportunity but also for the friendship along the years. Prof. Eduardo has been a true mentor who placed a significant amount of trust in me.

Secondly, I have to thank Eng. Gonçalo Silva and Doctor Pedro Morgado for the time invested in teaching me all the necessary tools to work and for always giving me helpful input and ideas.

I would also like to thank Prof. McCabe and the MUMS research group for allowing me the opportunity to work in the USA and for receiving me with open arms.

To my friends who during this work and academic journey were always capable of making me smile.

Lastly, I have to thank my family for giving me the support and the conditions all this years, despite my crazy ideas, to accomplish my objectives in every step of my life.

Abstract

The present work focus on studying the behaviour between fluorinated and hydrogenated mixtures that also strongly interact through hydrogen bonding. The excess viscosity of mixtures of fluorinated and hydrogenated alcohols have been shown to display large deviations to ideal behaviour when compared with mixtures of alcohols and mixtures of alkanes and perfluoroalkanes.

To further understand the underlying reasons beyond the presented negative excess viscosities, a computational study consisting of Molecular Dynamics (MD) simulations was performed for the mixtures (BuOH + HFB) and (HexOH + UFH), which was able to successfully reproduce the literature results. This study concluded that this behaviour results, possibly, from the unfavourable dispersion forces between the hydrogenated and fluorinated chains.

Molecular dynamics simulations were also used to calculate densities and excess volumes for three different systems, namely, (BuOH + HFB), (HexOH + UFH) and, (DOH + PFO). Also, diffusion coefficients were calculated for the (BuOH + HFB) mixture and the (HexOH + UFH) mixture.

Regarding the liquid structure, the simulations demonstrate the possible existence of segregation between hydrogenated and fluorinated chains and the presence of an nano structure consisting of an $H \cdots OH$ network for the (HexOH + UFH) mixture.

Lastly, the viscosity of 2,2,3,3,4,4,5,5,6,6,7,7,7-tridecafluoroheptan-1-ol was measured as a function of temperature between 283.15 K and 353.15 K.

Resumo

Este trabalho foca-se no estudo do comportamento de cadeias fluoradas e hidrogenadas que simultaneamente interagem através de pontes de hidrogénio. Anteriormente, foi reportado que as viscosidades de excesso de misturas de álcoois hidrogenados e fluorados apresentam grandes desvios à idealidade quando comparados com misturas de álcoois e misturas de alcanos e perfluoroalcanos.

De forma a compreender os mecanismos que provocam as viscosidades de excesso negativas, um estudo computacional constituído por simulações de Dinâmica Molecular foi executado para as misturas de (BuOH + HFB) e (HexOH + UFH), com este a reproduzir os resultados da literatura com sucesso. Este estudo concluiu que este comportamento é, possivelmente, devido às desfavoráveis forças de dispersão entre cadeias hidrogenadas e fluoradas.

Simulações de dinâmica molecular foram também utilizadas para calcular as densidades e os volumes de excesso de três sistemas diferentes, nomeadamente, (BuOH + HFB), (HexOH + UFH) e (DOH + PFO). Para além destes, os coeficientes de difusão foram calculados para a mistura de (BuOH + HFB) e a mistura de (HexOH + UFH).

Quanto à estrutura do líquido, as simulações demonstram evidências da existência de segregação entre as cadeias hidrogenadas e as cadeias fluoradas e a presença de uma nano estrutura constituída por uma rede de pontes de hidrogénio presente na mistura de (HexOH + UFH). Finalmente, a viscosidade de 2,2,3,3,4,4,5,5,6,6,7,7,7-tridecafluoroheptan-1-ol foi medida em função da temperatura entre 283.15 K e 353.15 K.

Contents

List of Tables

List of Figures

Nomenclature

Acronyms and Abbreviations

ECF - Electrochemmical Fluorination

MC - Monte Carlo

MD - Molecular Dynamics

OPLS - Optimized Potential for Liquid Simulation

AA - All Atom

rdf - Radial Distribution Function

H-bonds - Hydrogen Bonds

SD - Standard Deviation

ROM - Read-only Memory

Roman Letters

D - Diffusion Coefficient

k_B - Boltzmann Constant

M - Molar Mass

N - Number of particles

P - Pressure

$P_{\alpha\beta}$ - Off-diagonal Elements of the Pressure Tensor

q- Atomic Charge

T - Temperature

V - Volume

V_m^E - Excess Volume

x - Molar Fraction

Greek Letters

ϵ - Depth of the Potential Well

σ - Finite Distance at which the Inter-particle potential is zero

ρ - Density

η - Shear Viscosity

ξ - Correction to the energy interaction parameters

υ - Correction to the size interaction parameters

Molecules

BuOH - Butanol

HexOH - Hexanol

DOH - Decanol

HFB - 2,2,3,3,4,4,4-heptafluorobutan-1-ol

UFH - 2,2,3,3,4,4,5,5,6,6,6-undecafluorohexan-1-ol

PFO - 2,2,3,3,4,4,5,5,6,6,7,7,8,8,8-pentadecafluorooctan-1-ol

3:1 FTOH - 2,2,3,3,4,4,4-heptafluorobutan-1-ol

5:1 FTOH - 2,2,3,3,4,4,5,5,6,6,6-undecafluorohexan-1-ol

6:1 FTOH – 2,2,3,3,4,4,5,5,6,6,7,7,7-tridecafluoroheptan-1-ol

7:1 FTOH - 2,2,3,3,4,4,5,5,6,6,7,7,8,8,8-pentadecafluorooctan-1-ol

FTOH - Fluorotelomer alcohols

Chapter 1

Introduction

1.1 Fluorinated Compounds

Fluorine's property as the most electronegative element causes a tight biding with its valence electrons, resulting in low atomic polarizability and a small size. Also, the electronegativity difference between Carbon and Fluorine turns the C-F bond into a highly polar bond which contributes significantly to its strength. The combination of strong bonds and small size, gives fluorine an ability no other element possesses, to substitute hydrogen in virtually every kind of organic molecule.

Fluorinated compounds, such as perfluoroalkanes and its derivatives, are product of the mentioned distinctive properties of fluorine. They are carbon skeletons covered with fluorine "skins", synthesized by the substitution of the hydrogen atoms of a hydrocarbon chain for atoms of fluorine. This replacement of hydrogen by a substantially more electronegative element causes perfluoroalkanes to have properties and chemical behaviour that differ significantly from alkanes.

Consequently, mixtures of hydrogenated and fluorinated chains have shown a significant tendency for phase separation resulting in extensive regions of liquid-liquid immiscibility, large positive deviations from Raoult's law, and large positive excess properties, such as the excess enthalpy and volume. Generally, this behaviour has been interpreted has an alleged weak cross-

interaction between hydrogenated and perfluorinated chains leading to weak dispersion forces. This, alongside structural factors, such as the rigidity of fluorinated chains (as opposed to the characteristic flexibility of hydrogenated chains) and the incompatibility of cross-sectional diameters of hydrogenated and fluorinated chains contributes for the segregation between the perfluorinated chains and their counterparts.[17] [16]

Even though the scientific study of organofluorines started during the 19th century, it was only during the second world war that major breakthroughs were developed which allowed fluorinated compounds to be manufactured at a large scale, using the Fowler process or the Electrochemical Fluorination (ECF). After the war, the scientific interest on this compounds increased aiming to allow its civilian use, with the technology of ECF being acquired and implemented in a commercial plant for the production of fluorocarbons in 1951.[21] The study of the abnormal behaviour of solutions and mixtures of fluorinated compounds accompanied this developments with Scott extensively studying this systems during the 1950s and providing a wide screening of properties such as heat of mixing, vapour pressures, solubilities, and volume changes of mixing.[13]

1.1.1 Fluorinated Surfactants

Fluorinated surfactants are fluorocarbon-based surfactants that match the typical hydrophilic/hydrophobic surfactant behaviour to lyophobic behaviour towards hydrogenated organic medium. These traits come from the simultaneous presence of a fluorinated chain, which displays an intensified hydrophobicity compared to that of hydrogenated chains, and a poorly understood antipathy relatively to common hydrogenated solvents.[14]

Due to their enhanced ability to lower the surface energy of liquids and

solids, fluorinated surfactants have several applications as industrial substances, especially as detergents. Fluorinated surfactants are used as adjuvant components in fluoropolymer manufacture and processing, aqueous foams for fire extinction, formulations of herbicides, greases and lubricants, paints, polishes and adhesives.[14] They play a significant role in companies like Dupont and 3M with their stain repellent market being worth close to 1 billion annually and fluorosurfactants incorporated into polishes, paints and coatings worth 100 million per year.[26]

An obvious consequence of their usage are the higher emissions of fluorinated surfactants. And, because of their significant stability provided by their fluorinated backbone, they are increasingly being found in the environment, namely in animals in humans, since they are capable of accumulating through the food chain due to their hydrophobic character. This is a significant issue to public health since their toxicity has been proven and the removal of these compounds from aqueous solution is a difficult task.[24]

Nonetheless, the chain stiffness, which leads to a deficient molecular packing[16], and weak intermolecular forces[12] in fluorocarbon liquids, resulting in a high free volume, are responsible for the most exciting applications of fluorinated surfactants of different types and natures. Consequently, a high solubility of respiratory gases, which linked to their biocompability, turns them into the perfect liquid candidate for exciting procedures like drugs delivery in liquid ventilation context, as blood substitutes[18] and, in an environmental friendly application, as a potential system for CO_2 capture.[15]

Inside this class of surfactants, perfluorinated n-alcohols can be considered the simplest in terms of chemical structure. However, thermodynamic properties of these compounds are scarce, especially considering their interest in order to gain a further understanding of possible structural arrangements

and different types of molecular interactions. Moreover, like the more studied (alkane+perfluoroalkane) systems, mixtures of hydrogenated and fluorinated alcohols have also been shown to present deviations to ideal behaviour.

Thus, the role hydrogen bonding has on the thermodynamic properties of fluorinated and of hydrogenated alcohols has not been thoroughly studied in terms of liquid structure and molecular organization. As previously mentioned, hydrogenated and fluorinated segments are mutually phobic, therefore the addition of a polar alcoholic group to both these chains is expected to result in interesting behaviour due to the existence of associative interactions between two phobic segments. It has been suggested by Morgado[17] that these chains will try to create an $O \cdots HO$ network of hydrogen bonds formed between the hydroxyl head groups, surrounded by the carbon chain tails, which, in turn, segregate into hydrogenated and fluorinated domains so as to achieve the best packing possible for the phobic segments. This work will focus on studying thermodynamic properties of fluorotelomer alcohols, which are linear highly fluorinated molecules with a terminal OH group, described by the general formula, $CF_3(CF_2)_n(CH_2)_mOH$ (n+1:m FTOH). This fits a broader research effort of gaining knowledge about the properties of fluorinated substances and their mixtures in which experimental measurements, molecular simulation techniques and theoretical calculations have been used. Recently, experimental densities and viscosities of (2,2,3,3,4,4,4-heptafluorobutan-1-ol + Butanol) and (2,2,3,3,4,4,5,5,6,6,6-undecafluorohexan-1-ol + Hexanol) were reported which revealed large positive excess volumes and large negative excess viscosities. This work will mainly focus on studying the significant deviations to ideal behaviour of the transport properties of this mixtures and the possible existence of nano structures utilizing molecular dynamics simulations which are capable of

providing molecular insight on the reason beyond the reported experimental results. Experimental data for the viscosity of 2,2,3,3,4,4,5,5,6,6,7,7,7-tridecafluoroheptan-1-ol as a function of temperature will also be reported.

1.2 Computational Chemistry and Molecular Simulations

Alongside experimental data, molecular simulations are an incredibly useful complementary tool and, as they get perfected, a source of guidance for experimental trials. By not being dependable on the boundaries of nature, molecular simulations allow testing experimental conditions in a less expensive and time consuming way. It also enables researchers to better understand experimental observations and identify underlying mechanisms by providing a insight of the system at a molecular level. Thus, the insertion of this tool to explain the peculiar behaviour and large excess properties reported in the mixtures of hydrogenated and fluorinated alcohols was only logical.

Molecular simulations enable the detailed study of macroscopic thermodynamic properties, however, the selection of the computing technique is highly dependable on the type of properties being studied, which can be separated into the following categories: static equilibrium properties like density or potential energy of the system and dynamic properties - also known as non-equilibrium properties such as viscosity or diffusion.

Furthermore, the knowledge of an specific ensemble of a molecular configurations is never representative for the study of an thermodynamic property even if it is the ensemble with the global energy minimum. This occurs because the properties of a fluid can only be represented by the average of a wide range of representative statistical ensembles during a molecular simulation.

Therefore, any bona fide molecular simulation study must assure that the extracted properties come from an aggregate of molecular configurations with physical meaning. Ultimately, there are two methods of obtaining representative equilibrium ensembles of molecular systems: Monte Carlo simulations (MC)-not used in this work- and Molecular Dynamics simulations (MD).

1.2.1 Molecular Dynamics Simulations

The choice between Monte Carlo and Molecular Dynamics simulations is intrinsically related with the phenomena under investigation. In Monte Carlo simulations, at each stage a random move of a molecule is attempted. Depending on how favourable the energy change of the system with that move would be, the move is either accepted or declined. For the study of transport properties, intended in this work, MC simulations are the wrong option since they lack an objective definition of time. Furthermore, in the simulation of liquids, the large probability of the random move causing the overlap of two or more molecules and, consequently, the rejection of the mentioned move, decreases significantly the efficiency of this method sampling. Thus, MD simulations were the chosen method to this study.

In Molecular Dynamics simulations, a simulation engine numerically integrates Newtons laws of motion to move particles through time. This allows the observation of the system evolution during time and the calculation of its dynamic properties. To perform this integration it was used the Verlet algorithm.

$$v_i(t + \frac{1}{2}\delta) = v_i(t) + \frac{1}{2}\delta t a_i(t) \tag{1.1}$$

$$r_i(t + \delta t) = r_i(t) + \delta t v_i(t + \frac{1}{2}\delta t) \tag{1.2}$$

$$v_i(t+\delta t) = v_i(t+\frac{1}{2}\delta t) + \frac{1}{2}\delta t a_i(t+\delta t) \tag{1.3}$$

The ideal simulation of a certain system would be performed in a infinite system. Although, since MD simulations can only model a very small subset of a real physical system (on the order of nanometers), periodic boundary conditions are typically employed. As a particle "leaves" a simulation box, it re-enters on the opposite side, resulting in an infinite, yet periodic system. This approach avoids artifacts associated with hard boundaries, but may itself introduce artifacts associated with periodicity if the system is too small. Explicit self-interactions are not allowed; that is, you would not calculate the potential between a given particle and its periodic image.

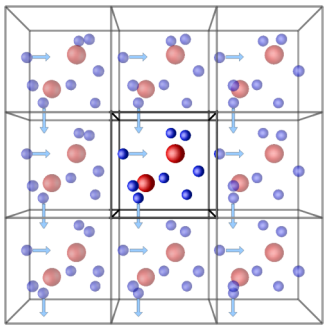

Figure 1.1: Periodic Boundary Conditions

The pair potential (Lennard-Jones) is based on the interactions of all the particles interacting with one another no matter how far they are separated from each other, hence, it should be noted that as the amount of particles increase, the performance will drastically decrease. However, as the distance between two particles increases, the potential energy between them asymptotically approaches zero. Therefore, commonly a certain distance, r, is defined, as the limit which the potential energy between two particles is relevant. This means that it is not necessary to determine all the interac-

tions between particles but instead only the ones separated with a distance inferior to r. These interactions will contribute a negligible amount in the overall potential energy of the system and excluding them can increase performance. Neighbour lists can be thought of as the local neighbourhood of important particles for each particle in the system. Usually much smaller than the total number of particles present, these are the only particles that need to be accounted for when evaluating the interaction energies. There are several algorithms to stablish this neighbour lists. The one used in this work is the Verlet list.

1.2.2 Force Field - OPLS

A force field is a mathematical expression chosen to describe the intra- and inter-molecular potential energy of a collection of atoms, and the corresponding parameters that will determine the energy of a given ensemble.[3]

Ideally, a force field would be able to comprise all sorts of interactions between different molecules in a system, in order to successfully reproduce the system's macroscopic properties. However, besides taking into account the interactions between pairs of molecules, that would also require considering the alteration of such interactions by adding another molecules, the so called n-body problem. So far, a solution for this problem is still unknown, and even its simplest form, the three-body problem, is only addressed by numerical analysis approximations. Therefore, the effort to consider more than the pair interactions, would either be extremely demanding computational wise or just impossible.

Consequently, the construction of a force field obliges to employ significant physical approximations in order to describe the intermolecular interactions. Usually, these functions and parameters are derived from experimental work

on single molecules and from accurate quantum mechanical calculations and, afterwards, are refined by the use of computer simulations to match the obtained macroscopic properties with experiment. This process is called parametrisation and it is what makes the force fields and its parameters empirical since depending on the procedure followed to develop them and the set of input data used to optimize their parameters, different force fields applicable to different systems or problems are obtained.[7]

Also, as mentioned by its definition, a force field needs to describe both the intermolecular interactions and the intra-molecular interactions existent in a system. Logically, the parameters used to do it are divided in bonded parameters, which describe the intra-molecular contributions and non-bonded parameters which account for the intermolecular contributions.

Intra-molecular terms

The intra-molecular or local contributions to the total energy include bond stretching, angle bending and dihedral torsions. Bond stretching and angle bending are usually represented using a simple harmonic function that controls the length of covalent bonds and the distance between the two external atoms forming the angle, respectively. In any molecule containing more than four atoms in a row, it is also necessary to include a dihedral or torsional term. The summation of this terms results in the following expression:

$$U = \sum_{bonds} \frac{1}{2} k_b (r - r_0)^2 + \sum_{angles} \frac{1}{2} k_a (\theta - \theta_0)^2 + \sum_{torsions} \frac{Vn}{2} [1 + \cos(n\Phi - \delta)] \quad (1.4)$$

where r_0 and k_b are stretching and bending constants, respectively; k_a is the equilibrium bond length and θ_0 is the equilibrium angle. Torsional energy

is usually represented by a cosine function, where Φ is the torsional angle, δ is the phase, n defines the number of minima or maxima between 0 and 2π (also called multiplicity) and, V_n determines the height of the potential barrier. While angle bending and bond stretching are high frequency motions which often are not relevant for the study of the properties of interest and can be replaced by a rigid approximation, torsional motions are necessary to ensure the correct degree of rigidity of the molecule and to reproduce major conformational changes due to rotations about bonds. Hence, they play a crucial role in determining the relative stability of different molecular conformations.[7]

Intermolecular terms

Starting with the non-bonded terms, Van der Waals interactions arise from the balance between repulsive and attractive forces. The physical origin of the attraction lies in the dispersion forces generated between instantaneous dipoles, which arise from fluctuations in electronic charge distributions in all molecules, as first explained by London. The repulsion is due to the overlap of the electron clouds of both atoms.[3] The 12-6 Lennard-Jones (LJ) potential is very often used to represent these interactions:

$$V(r) = 4\epsilon\left[\left(\frac{\sigma}{r}\right)^{12} - \left(\frac{\sigma}{r}\right)^{6}\right] \tag{1.5}$$

in which the first term represents the repulsive part of the potential while the second is the attractive term. The ϵ is depth of the potential well and a measure of how strongly the two particles attract each other, σ is the finite distance at which the inter-particle potential is zero and provides a measurement of how close two non-bonding particles can get and, r is the

distance between particles.

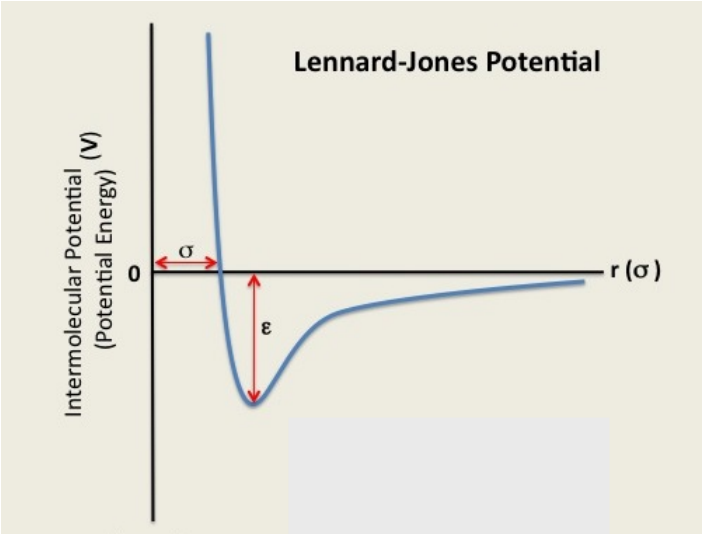

Figure 1.2: The Lennard-Jones potential

The final term of the non-bonded parameters serves to describe the electrostatic interactions. The electrostatic interaction arises due to the unequal distribution of charge in a molecule. Within the force field framework this uneven distribution of charge can be modelled by placing point charges at each of the atomic sites. Due to charge conservation for a neutral molecule these sum to zero. The interaction between these point charges is generally modelled by a Coulomb potential:

$$V(r) = \sum_i \sum_{j \neq i} \frac{q_i q_j}{4\pi\epsilon_0 r_{ij}} \tag{1.6}$$

where ϵ_0 is the permittivity of free space, q are atomic charges and, r_{ij} is the distance between nuclei i and j. The determination of the partial charges that reproduce the electrostatic properties of molecules are commonly obtained from *ab initio* calculations and then deriving them from the quantum mechanical potential.[7]

Chapter 2

Experimental Procedure

The 2,2,3,3,4,4,5,5,6,6,7,7,7-tridecafluoroheptan-1-ol (6:1 FTOH, CAS number: 375-82-6) was purchased from Apollo Scientific, for which was claimed a 97% purity. Prior to experimental measurements, the 6:1 FTOH was dried with VWR Prolabo 4A molecular sieves to a maximum water content of 200 ppm (analysed by Karl-Fischer coulometry).

The viscosity of 6:1 FTOH was measured in the temperature range of 283.15 K and 253.15 K at atmospheric pressure using an automated SVM 3000 Anton Paar rotational Stabinger viscosimeter-densimeter. The measuring principle for this instrument in based on a tube(outer rotor) filled with sample liquid rapidly rotating at constant speed and a inner hollow measuring rotor. Because of its low density, the rotor is centered in the heavier liquid by buoyancy forces. The rotor is forced to rotate by shear stresses in the liquid and is guided axially by a built-in permanent magnet. The rotating magnetic field delivers the speed signal and induces eddy currents in the surrounding copper casing. These eddy currents are proportional to the speed of the rotor and exert a retarding torque on the rotor.

Two separate torques influence the speed of the measuring rotor, the viscosity-dependent driving torque, which is proportional to the speed difference between the outer tube and the inner rotor, and the retarding torque caused by eddy currents, which is proportional to the inner rotor speed. At equilibrium, the two torques are equal and the viscosity measurement can,

therefore, be traced back to a single speed measurement.

The integrated thermostat with cascaded Peltier elements and Pt-100 thermometer as well as the low thermal mass of the measuring cell enable rapid changes and exact adjustments to the measuring temperature which assures a fast and efficient thermal stability. The temperature uncertainty is ±0.02 K from 288.15 to 378.15 K. The precision of the dynamic viscosity measurements is ±0.5%.

Chapter 3

Simulation procedure and details

Molecular dynamics simulations were performed to gain insight on the behaviour of the (hydrogenated + fluorinated) alcohol systems on a molecular level by applying models based on the atomistic optimized potential for liquid simulations all-atom (OPLS-AA) force field.[10] All the necessary potential parameters for Butanol were published in the original OPLS-AA papers[10][28], while for Hexanol and Decanol the parameters are published in the L-OPLS-AA papers, namely the extension for alcohols.[25]

To describe the fluorinated alcohols, 3:1 FTOH, 5:1 FTOH and 7:1 FTOH the model used in this work was built by using the force-field parameters of the $(-CF_2 - CH_2 - OH)$ segment from the model of Trifluoroethanol developed by Duffy [4] and for the perfluoroalkyl "tail" $(-CF_3 - CF_2-)$ from the OPLS-AA work on perfluoroalkanes.[28] The remaining dihedral torsion parameters were taken from the work of Padua[22], and the partial charge of the carbon atom in the first $-CF_2$ group was adjusted to give the molecule a net zero. Table 3.1, comprises all the non-bonded parameters used to for the construction of the mentioned molecules.

According to the OPLS parametrization, the non-bonded Lennard-Jones interactions between different types of sites were calculated using the geo-

metrical mean rule for both size and energy:

$$\epsilon_{ij} = \sqrt{\epsilon_{ii}\epsilon_{jj}} \tag{3.1}$$

$$\sigma_{ij} = \sqrt{\sigma_{ii}\sigma_{jj}} \tag{3.2}$$

The cross-interaction energy and the cross-interaction diameter between alkyl hydrogen atoms and perfluoroalkyl fluorine atoms were allowed to depart from the geometrical mean to capture the weak unlike interactions between hydrogenated and fluorinated chains and match the experimental excess properties. For this purpose, it was introduced corrections to the energy and size binary interaction parameters, $\xi = 0.80$ and $\upsilon = 1.035$, for (BuOH + HFB) as suggested by Morgado for the OPLS-AA force field [17] and $\xi = 0.77$ and $\upsilon = 1.035$ for (HexOH + UFH) in the L-OPLS-AA force field.

In the same molecule, only sites separated by three or more bonds count for the non-bonded interactions between sites. Non-bonded interactions between sites separated by three bonds are scaled by a factor of 0.5.

All MD simulations were carried out with the open-source package GROMACS (version 2018)[1][27], in cubic boxes with periodic boundary conditions imposed in all directions and a time step of 2 fs. All bonds involving Hydrogen atoms were treated as rigid by being constrained to their equilibrium lengths, using the LINCS algorithm.[9] Simulations were conducted for systems composed of 300 molecules for (HexOH + UFH) and (DOH + PFO) and, 500 molecules for (BuOH + HFB) with the system size being conserved as the molar ratio of alcohol to fluorinated alcohol was changed. The temperature was controlled with the Nosé-Hoover thermostat [20] and in the NPT emsembles, at 1 atm, the Parrinello-rahman barostat[23] was im-

plemented. The general simulation scheme was the following: Initially, the molecules were placed randomly in the box and were allowed to equilibrate in the NPT ensemble for 2.5 ns, during this period, the density of the system converged to mean values, then a 2.5 ns long production run is performed from which the density of the system could be calculated. Afterwards, 2 ns long equilibration runs were performed in the canonical (NVT) emsemble at densities obtained from NPT simulations at atmospheric pressure which are followed with NVT production runs from 5-50 ns long which allow the calculation of transport properties such as diffusion coefficient and viscosity. The significant difference between some simulation runs is justified by the fluorinated alcohols having much slower molecular dynamics than alcohols.

In all simulations, a neighbour list, with a radius of 10 Å, was used and updated every 10 time steps. Both non-bonded Lennard–Jones and electrostatic potential were truncated by using cut-offs of 14 Å, respectively and analytical tail corrections to dispersion terms were added. The long-range electrostatic (coulombic) interactions beyond the cutoff were calculated using the particle-mesh Ewald (PME) method. Before the molecular dynamics runs, the boxes were subjected to energy minimization by the steepest descent method with a maximum number of steps of 25000.

Table 3.1: Non bonded parameters present in the forcefield and used for the construction of BuOH, HexOH, DOH, HFB, UFH and PFO

Name	Bond Type	M	q	ϵ	σ
opls_135	CT	12.0110	-0.180	0.350	0.276144
opls_136	CT	12.0110	-0.120	0.350	0.276144
opls_140	HC	1.0080	0.060	0.250	0.125520
opls_154	OH	15.9994	-0.683	0.312	0.711280
opls_155	HO	1.0080	0.418	0.000	0.000000
opls_157	CT	12.0110	0.145	0.350	0.276144
opls_160	CT_4	12.0110	0.126	0.350	0.276144
opls_161	CTF	12.0110	0.532	0.325	0.259408
opls_162	OH	15.9994	-0.635	0.307	0.711280
opls_163	HO	1.0080	0.429	0.000	0.000000
opls_164	F	18.9984	-0.206	0.294	0.255224
opls_165	HC	1.0080	0.083	0.250	0.125520
opls_961	CTF	12.0110	0.360	0.350	0.276144
opls_962	CTF	12.0110	0.240	0.350	0.276144
opls_965	F	18.9984	-0.120	0.295	0.221752
lopls_966	CTL	12.0110	-0.222	0.350	0.276144
lopls_967	CTL	12.0110	-0.148	0.350	0.276144
lopls_968	HTL	1.0080	0.074	0.250	0.125520
lopls_969	HTL	1.0080	0.074	0.250	0.110000

3.1 Calculation of thermodynamic properties from MD Simulations

The calculation of viscosities from MD simulations is not a straightforward process since it does not have a general accepted methodology and, there not many tools available for its calculation considered reliable. This happens because its not a common property to obtain from MD simulations and the literature available, usually, does not make a detailed description of the process for its calculation. Therefore, a significant part of this work consisted on understanding the proper method to calculate viscosities. Subsequently, some important remarks were taken from this experience.

Due to its simplicity, the Green-Kubo relation based equilibrium molecular dynamics (MD) simulations is perhaps the most widely used method to calculate viscosities. In this approach, the shear viscosity is calculated from the integral over time of the pressure tensor autocorrelation function

$$\eta = \frac{V}{k_B T} \int_0^\infty \langle P_{\alpha\beta}(t) \cdot P_{\alpha\beta}(0) \rangle dt \tag{3.3}$$

where V is the system volume, k_B is the Boltzmann constant, T is temperature, $P_{\alpha\beta}$ denotes the off-diagonal elements of the pressure tensor, and the angle bracket indicates the average ensemble. Plus, in order to reduce the statistical uncertainty, to the average of the off-diagonal elements of the pressure tensor P_{xy}, P_{xz} and P_{yz} was added the equivalent $\frac{P_{xx}-P_{yy}}{2}$ and $\frac{P_{yy}-P_{zz}}{2}$, because of rotational invariance.[19]

A time step of 1 femtosecond and 2 femtosecond were tried for the execution of this simulations. It was concluded that with both time steps the energy of the system was conserved through out the simulation, as expected.

However, the step at which the energy of the system is registered has an important role on the description of the autocorrelation function of pressure tensors. The figure depicted below, figure 3.1, shows the autocorrelation function of a pressure tensor when the energy of the system is registered with a step of 1 femtosecond, 2 femtosecond and 20 femtosecond. Clearly, the integral of the autocorrelation function is defined by short correlation times since this function very quickly tends to zero. Therefore, its essential to assure that this function is as accurate as possible in this small window, which does not happen when the energy of the system is tracked every 20 femtoseconds. Meanwhile, the difference between storing the energy of the system every 1 femtosecond or 2 femtosecond is practically non existent thus, 2 femtoseconds are the best compromise between accuracy of the autocorrelation function and the used ROM.

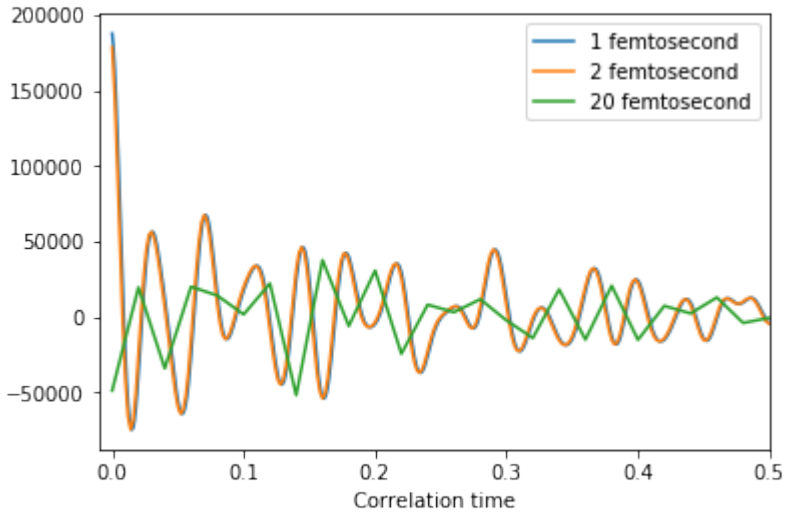

Figure 3.1: Autocorrelation function when storing the energy of the system every 1 femtosecond, 2 femtosecond or 20 femtosecond

Also, theoretically, the pressure tensor autocorrelation function decays to zero in the long time limit and the integral should reach a constant value,

which corresponds to the calculated shear viscosity. In practice, however, due to the accumulation of noise at long times the integral does not necessarily converge to a constant value, but instead shows fluctuations at long times. Hence, to solve this issue it was used the methodology proposed by Zhang [29], which allows for the visualization of a more clear finite plateau region. As proposed by it, 40 independent NVT trajectories at a given temperature were performed and, for each of them, was calculated the shear viscosity based on the Green-Kubo relation. Afterwards, the average and standard deviation of all the running integrals was calculated with the average running integral being fitted to the following double-exponential function with the weight of $1/t^b$

$$\eta = A\alpha\tau_1(1 - \exp^{-t/\tau_1}) + A(1 - \alpha)\tau_2(1 - \exp^{-t/\tau_2}) \tag{3.4}$$

and the average standard deviation fitted to the power law function

$$SD(t) = At^b \tag{3.5}$$

For the determination of the cutoff time with was used the proposed $SD = 0.4\langle\eta\rangle$. Figure 3.2 shows the shear viscosity of 40 independent NVT trajectories and clearly shows the fluctuations previously mentioned with no clear plateau individually, while the average obtained from the 40 independent NVT trajectories has a clear plateau.

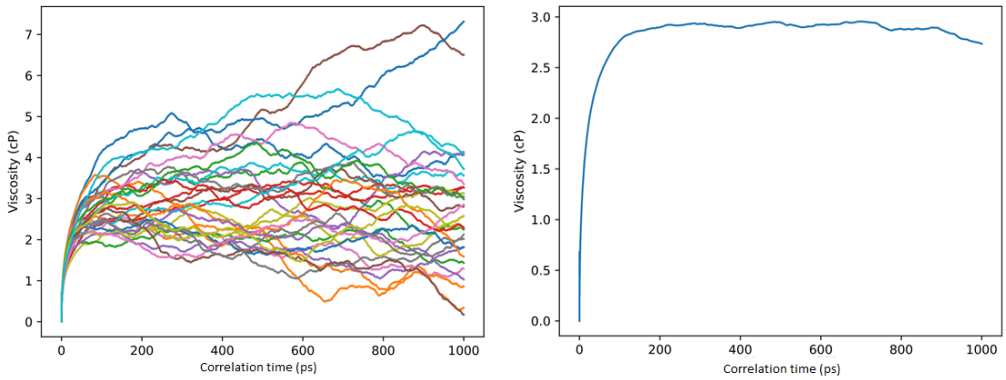

Figure 3.2: Shear viscosity of 40 independent NVT trajectories and the corresponding average for UFH at 343.15 K

The length of such trajectories went from 5 ns to 50 ns, since no specific criteria was mentioned in the article. Mondello and Crest[16] proposed that the simulations should be ran for between 100 and 200 times the rotational relaxation time of the molecule. However, UFH and HFB have very slow molecular dynamics and, consequently, high rotational relaxation times, therefore, this criteria does not match with performing 40 independent NVT trajectories since it places too much effort on ROM. So, on this work, the criteria for how long the simulation were ran was based on a compromise between the proposed by Mondello and Crest and the available ROM.

An high degree of automation was required for the construction of the systems and for the scheduling of the workflow. For this purpose, the Mosdef-Hub was crucial since it allowed an easy construction of the molecular systems by using mBuild and Signac-Flow for the organization and realization of the simulations workflow.[2][8][11]

Despite the main concern of this work being the calculation of viscosities, other properties were extracted from the performed simulations, not only to validate them but also to support further conclusions.

Regarding the system densities, they were collected directly from the average values of the box volume in the NPT production samplings.

The diffusion coefficients of different mixtures were calculated from the linear part of the mean square displacement of the center of mass of the solute molecules according to the Einstein equation:

$$D = \frac{1}{6N} \lim_{t \to \infty} \frac{d}{dt} \sum_{i=1}^{N} < [r_i(t) - r_i(0)]^2 > \tag{3.6}$$

where $[r_i(t) - r_i(0)]^2$ is the mean square displacement of the solute and the brackets stand for average over time. The summation extends to all solute molecules in the simulation. The final value of diffusion coefficient was obtained from the average of 5 values obtained independently.

Furthermore, effective radii were calculated using the diffusion coefficients obtained via MD simulations and experimental viscosities reported in literature[5] since the calculated viscosities have, within, an high degree of uncertainty.

The translational motion of a solute in a fluid solution at infinite dilution can be described by the Einstein equation

$$D = \frac{k_B T}{\zeta} \tag{3.7}$$

where D is the diffusion coefficient, k_B is the Boltzmann constant, T is the absolute temperature, and ζ is the friction coefficient. At the hydrodynamic limit of a sphere of radius r diffusing in a fluid having a shear viscosity η, one can recover the Stokes-Einstein relation.

$$D = \frac{k_B T}{C \pi \eta r} \tag{3.8}$$

where the constant C is determined by the boundary conditions and is equal to 6 for the case of "stick" boundary conditions.

Chapter 4

Results and Discussion

4.1 Densities and Excess Volumes

The densities were calculated for (BuOH + HFB), (HexOH + UFH) and (DOH + PFO) at 298.15 K . In the figure 4.1, (BuOH+HFB) at 298.15 K, is plotted and compared with experimental data[17]. Both (HexOH + UFH) and (DOH + PFO), in the figure 4.2 and 4.3, respectively, at 298.15 K, are displayed and compared with unpublished experimental measurements.

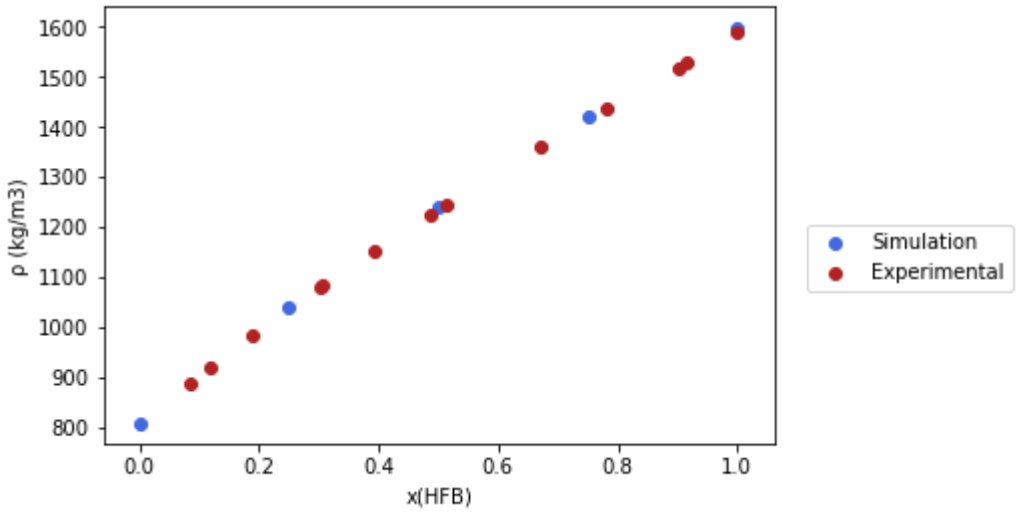

Figure 4.1: Densities of (BuOH + HFB) at 298.15 K

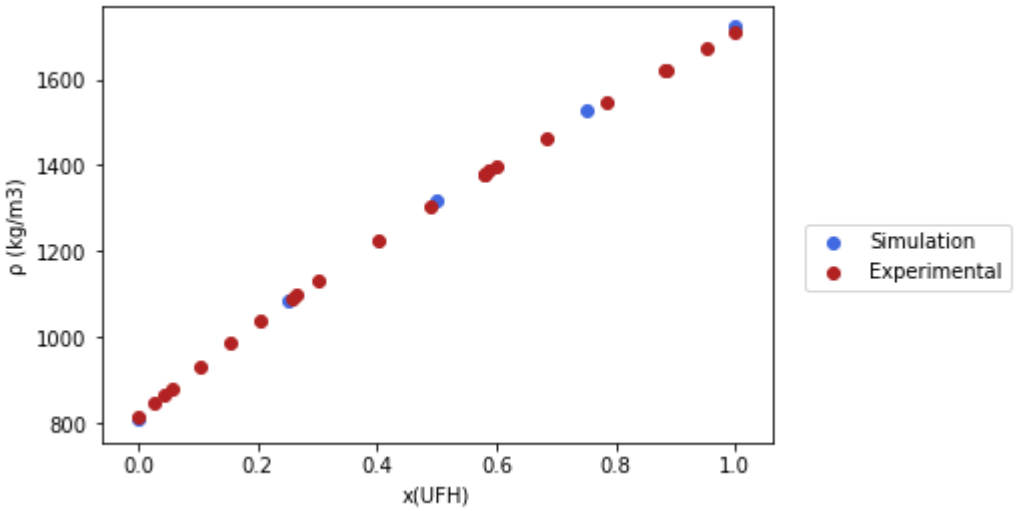

Figure 4.2: Densities of (HexOH + UFH)at 298.15 K

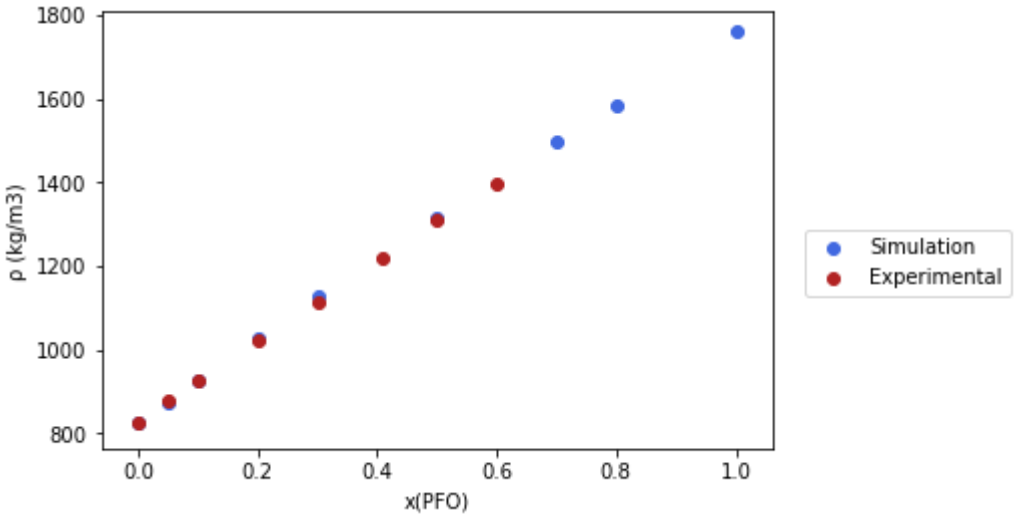

Figure 4.3: Densities of the mixture PFO + Decanol at 298.15 K

This plots demonstrate a good agreement between the experimental and the calculated densities, which validates the models used in this molecular simulations. Subsequently, the related excess volumes were calculated and plotted in figures 4.4 and 4.5. Again, for the (BuOH + HFB) the values were

compared with the experimental data[17] while the (HexOH + UFH) system were compared with unpublished experimental measurements.

$$V_m^E = \frac{x_1 M_1 + x_2 M_2}{\rho_{12}} - \frac{x_1 M_1}{\rho_1} - \frac{x_2 M_2}{\rho_2} \tag{4.1}$$

As previously mentioned, to model the unlike $H - F$ interaction, the corrections on size and energy parameters proposed by Morgado[17], $\xi = 0.8$ and $\upsilon = 1.035$, were introduced in the forcefield for the (BuOH + HFB) mixture. As expected, the values calculated for excess volume from MD simulations for this system demonstrate a good agreement with the experimental data and successfully reproduce the symmetry of the experimental curves. In the same paper, Morgado had already been able to successfully utilize this corrections to reproduce the excess volumes of this system.

However, when the parameters modelled for (Hexane + Perfluorohexane) in the L-OPLS force field, $\eta = 1.035$ and $\upsilon = 0.77$, were applied to the mixture of (HexOH + UFH) despite presenting the symmetry of the experimental curves, the calculated excess volumes are significantly lower than the ones experimentally obtained. Accordingly, simulations were ran to parametrize the best correction for the (HexOH + UFH). The results are given below on figure 4.5. From this results is possible to draw the conclusion that to correctly reproduce the experimental excess volumes of the (HexOH + UFH) system, $\eta = 0.77$ and $\upsilon = 1.039$ must be used as the correction.

This same correction was kept for the (DOH + PFO) system. However, PFO is soluble in Decanol up to x(PFO)=0.6, at room temperature. Above this composition, (solid + liquid) phase separation is observed. As so, instead of comparing excess volumes, the calculated and experimental molar volumes were compared, figure 4.6.

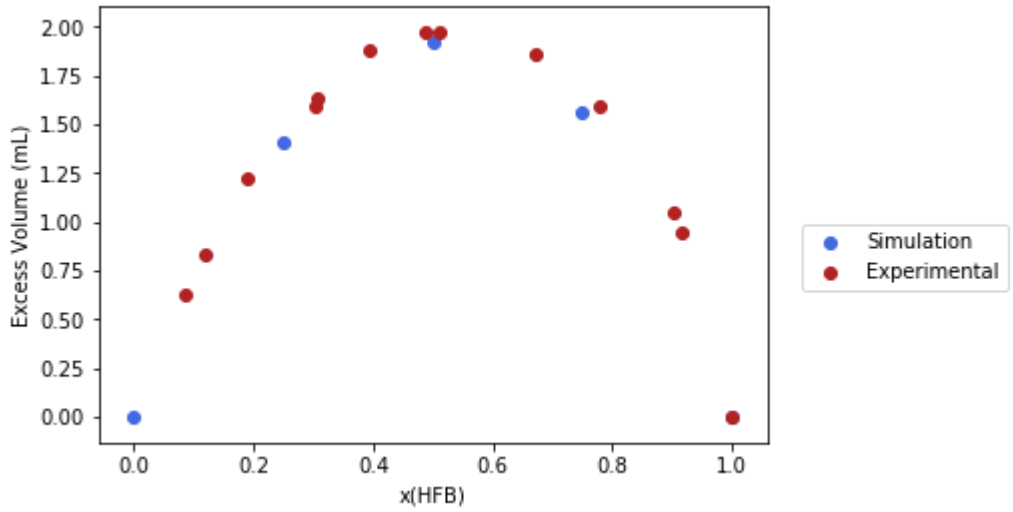

Figure 4.4: Excess Volumes of (BuOH + HFB)

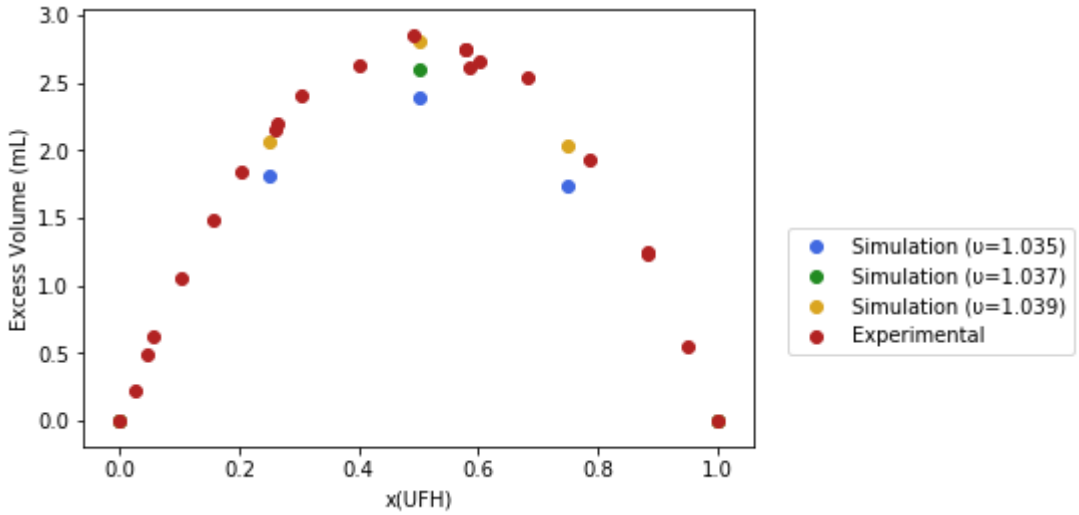

Figure 4.5: Excess Volumes of (HexOH + UFH)

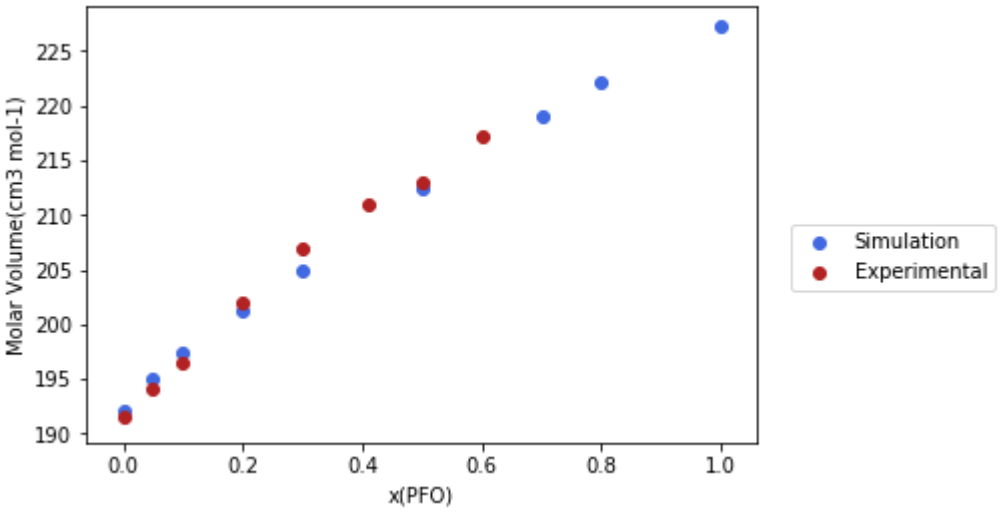

Figure 4.6: Molar Volume of the mixture (PFO + Decanol) at 298.15 K

4.2 Viscosities and Excess Viscosity

4.2.1 Pure compounds

The experimental measures of the viscosity of 6:1 FTOH as function of temperature are reported in table A.1, presented in appendix A and plotted in the figure 4.7, alongside other different fluorotelomer alcohols. As expected, the viscosities of fluorotelomer alcohols increase with the increase in chain length. As far as known, this are the first reported viscosities for 6:1 FTOH, and they seem to be in line with previous measurements of other fluorotelomer alcohols. The calculated viscosities, from MD simulations, of HFB and UFH at 293.15 K, 313.15 K and 343.15 K for UFH are also displayed in figure 4.7. Clearly, the MD simulations are capable of reproducing the variation viscosity has with the increase in temperature.

Also, to place in context the viscosity data of fluorotelomer alcohols, literature data about the viscosity of different families of compounds, but with structural similarities to fluorotelomer alcohols, were collected and plotted in figure 4.8. The higher viscosity of fluorotelomer alcohols in relation to the other compounds is explained by the presence of hydrogen bonds, causing a resistance on the molecules ability to flow, combined with the higher molecular weight of Fluorine which is also responsible for perfluoroalkanes higher viscosity, compared to alkanes.[6]

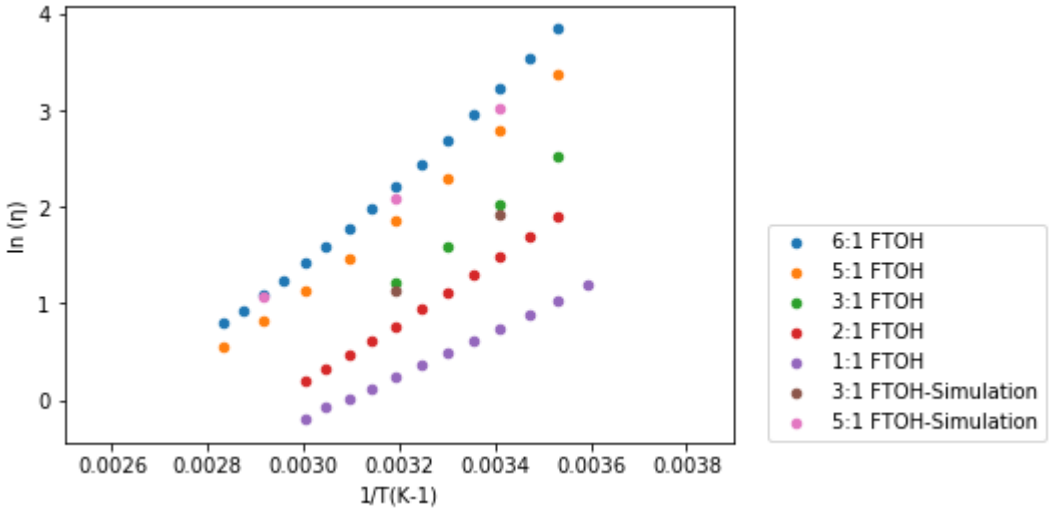

Figure 4.7: Experimental and calculated viscosities of fluorotelomer alcohols as a function of temperature

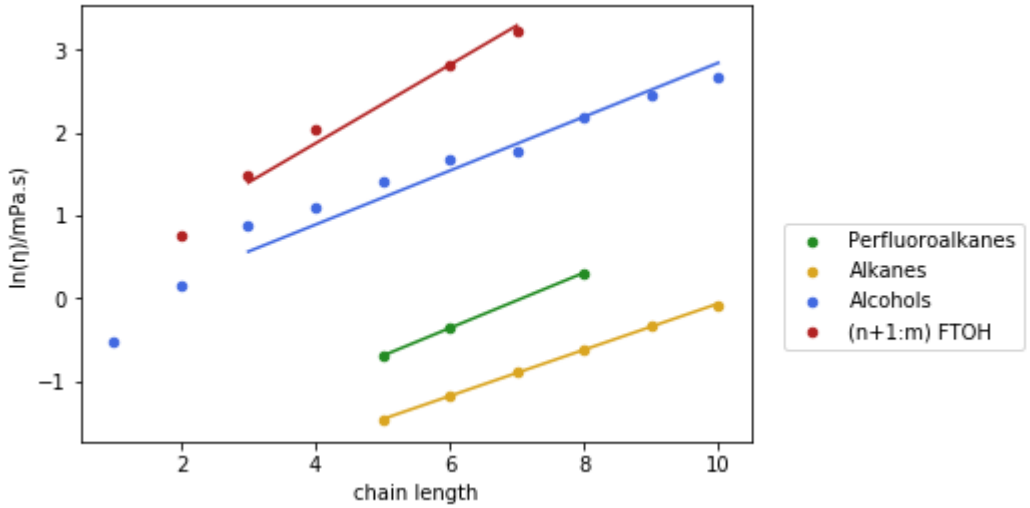

Figure 4.8: Experimental viscosities at 293.15 K

4.2.2 Mixtures

The calculated viscosities for the (BuOH + HFB) mixture are plotted in the Figure 4.9 and the (HexOH + UFH) mixture in the Figure 4.10, at 293.15

K. Both were compared with experimental viscosities present in literature.[5] In Appendix B, are the calculated viscosities and excess viscosities for both systems and the plots with the experimental comparison for the remaining temperatures, 313.15 K and 343.15 K.

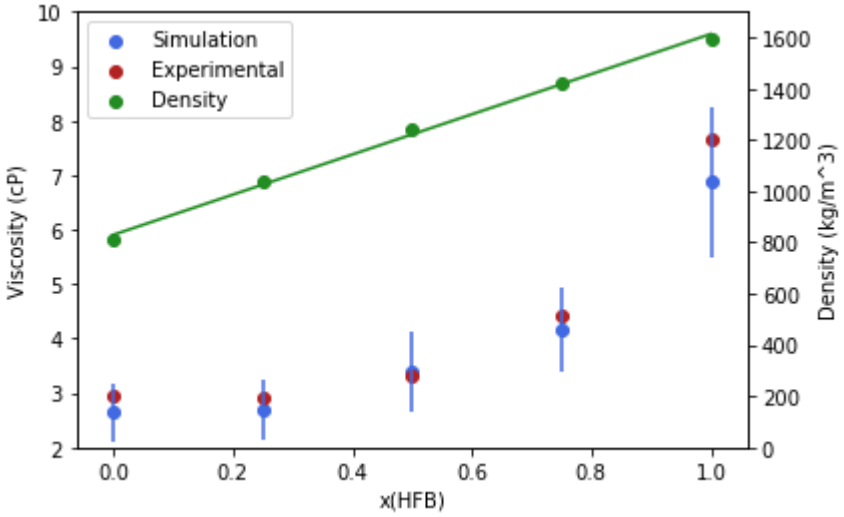

Figure 4.9: Experimental and simulated viscosities of (BuOH + HFB) and simulated densities at 293.15 K

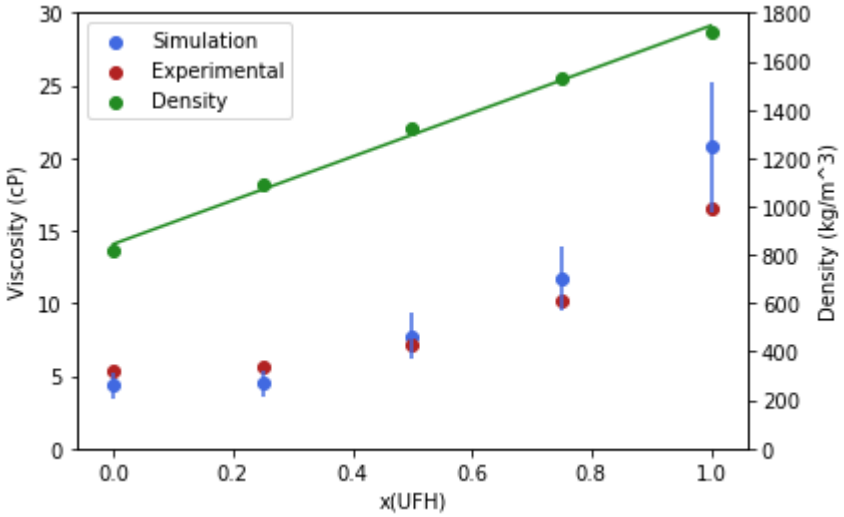

Figure 4.10: Experimental and simulated viscosities of (HexOH + UFH) and simulated densities at 293.15 K

Calculating viscosities from MD simulations has an inherent high degree of uncertainty for the reasons previously explained, nonetheless, all the experimental data is inside the uncertainty range of the calculated viscosities. Moreover, is interesting to verify that the simulations predict the singular excess behaviour of viscosity in this mixtures, showing results close to the experimental and revealing large negative deviations as shown in figure 4.11 and figure 4.12. This important step reveals that the simulation scheme and the models used are capable of reproducing the measured behaviour for (BuOH + HFB) and (HexOH + UFH).

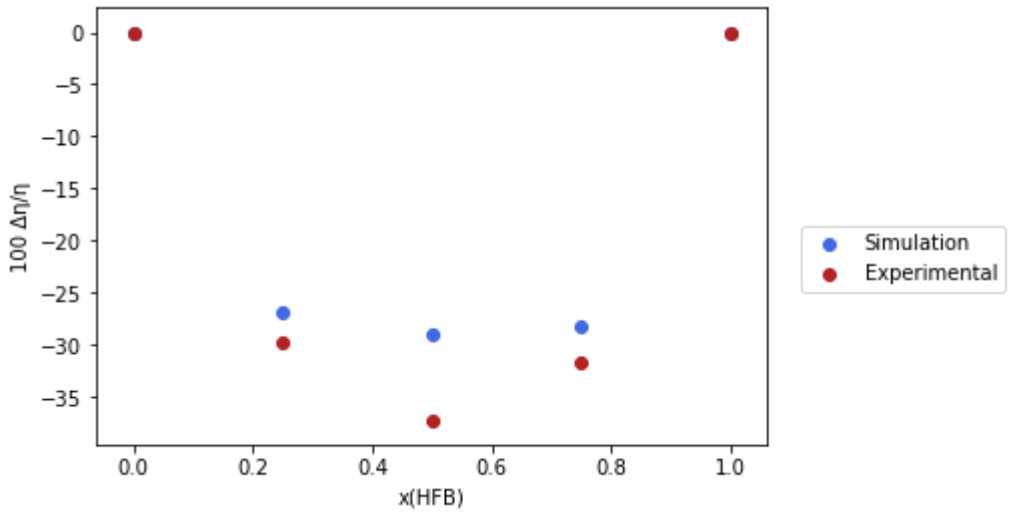

Figure 4.11: Experimental and simulated excess viscosities for (BuOH + HFB)

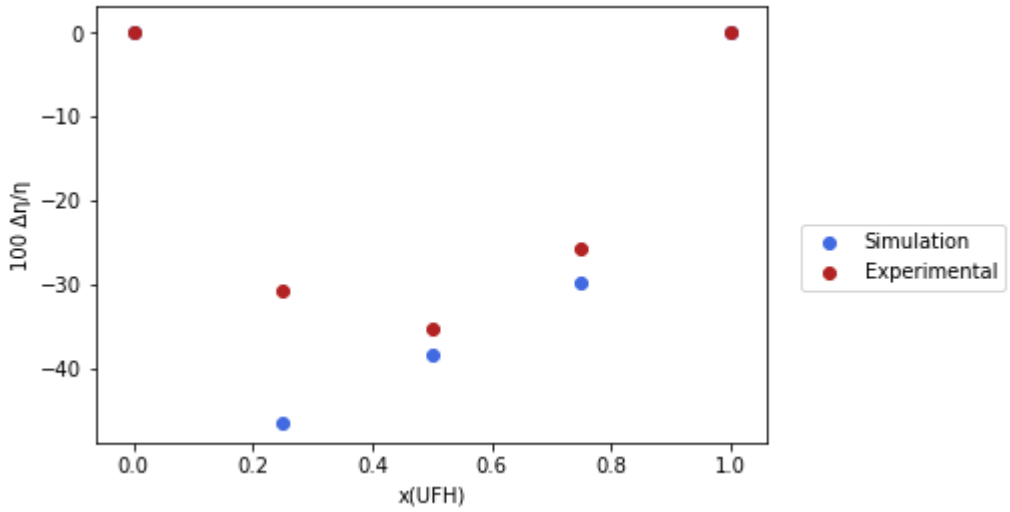

Figure 4.12: Experimental and simulated excess viscosities for (HexOH + UFH)

The comparison between the reported experimental excess viscosities for (BuOH + PFBuOH) and (HexOH + UFH) and other mixtures of compounds with similarities, figure 4.13, highlights some of the possible reasons beyond the noted behaviour: (i) As seen by the contrast between the (Butanol +Pentanol and Nonanol + Decanol) mixtures and the (Butanol + Nonanol and Butanol + Decanol) mixtures, the mixing of two different compounds generates a deviation from the ideal mixture, however, when the viscosities of the components are significantly different from each other there is a large increase in the negative variation of the excess viscosities. (ii) The weak dispersive interactions and the repulsive part of the intermolecular potential are responsible for a weaker interaction between hydrogenated and fluorinated chains which causes a more fluid flow when both these chains are mixed together and explains the (Perfluorohexane + Hexane) excess viscosity. (iii) In case of the (Decane + Hexanol) mixture, the addition of a alkane to a alcohol decreases the overall amount of hydrogen bonds in the system leading to the

mixtures having a large negative deviation to ideal behaviour.

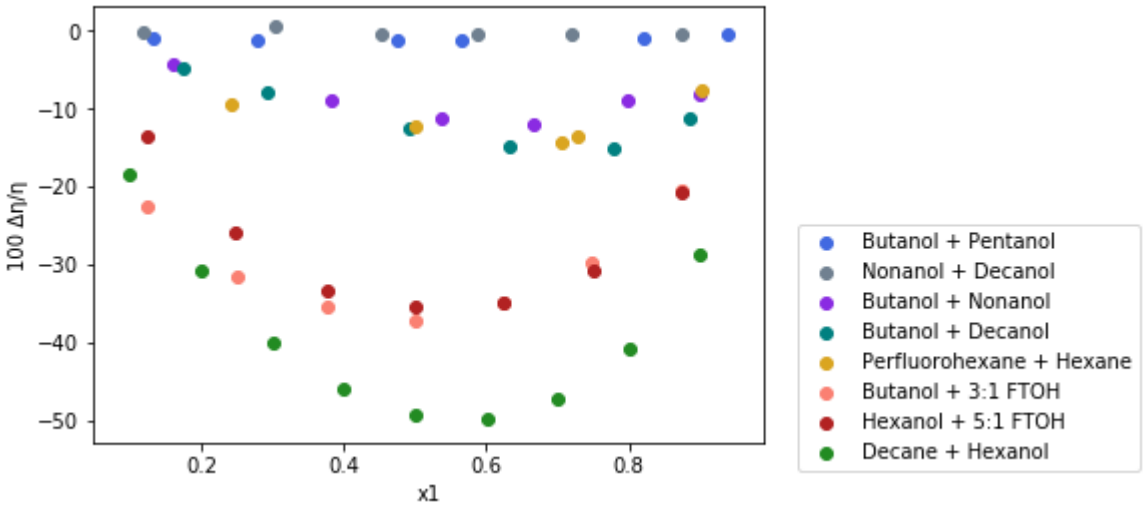

Figure 4.13: Experimental excess viscosities

Bearing in mind these considerations, other transport properties namely, the diffusion coefficients and effective radii were obtained to better understand the movement and motion of this molecules in the mixture.

4.3 Diffusion Coefficients and Effective Radii

The calculated diffusion coefficients for BuOH and HFB in (BuOH + HFB) and, HexOH and UFH in (HexOH + UFH) at 293.15 K and 343.15 K are shown in the following figures and presented in table C.2 and C.1 in Appendix C. No experimental or simulation data on these mixtures were found reported previously.

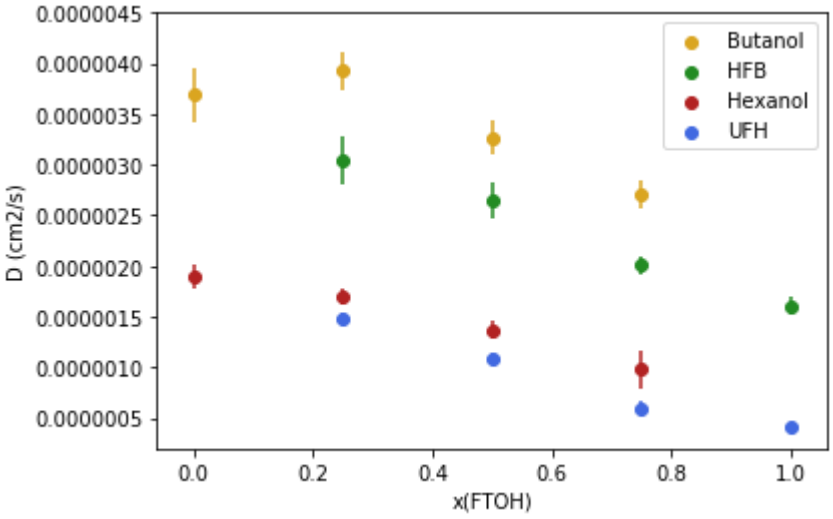

Figure 4.14: Diffusion coefficients at 293.15 K for (BuOH + HFB) and (UFH + Hexanol)

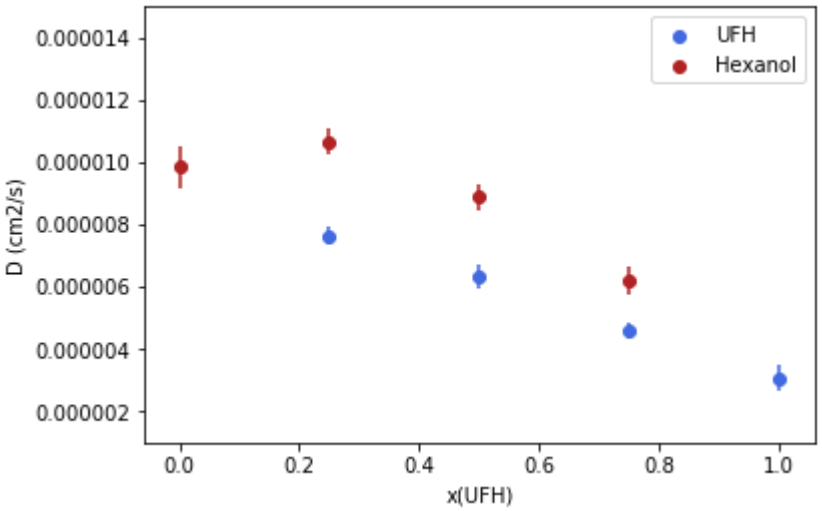

Figure 4.15: Diffusion coefficients at 343.15 K for (UFH + Hexanol)

Since the FTOH viscosities are higher than that of alkanols, it was expected for the diffusion coefficients to decrease with the increase of x(FTOH). Also, lower diffusion coefficients of FTOH in comparison to the alkanols occur because FTOH molecules are bulkier, due to the bigger size of Fluorine against Hydrogen, which makes their movement in the mixture more difficult.

To try gaining a further understanding of the molecules motion in the mixtures an attempt was made to calculate an effective radius, using the Stokes-Einstein equation, valid for an incompressible Newtonian fluid, as explained in section 3.1. This property allows a better evaluation of the motion of the molecules in the different mixtures as it cancels the effect of different viscosities on their movement. A higher effective radius means the motion of the molecule in the mixture is more difficult. The results are plotted in figure 4.16

Simulations of HexOH and UFH at infinite dilution in UFH and HexOH, respectively, were also performed and the corresponding diffusion coefficients and effective radii calculated. These are included in figure 4.16. Figure **??**

consisted of a single molecule of hexane and a single molecule of perfluorohexane inserted in pure hexanol, pure UFH and an equimolar mixture. This allows understanding the influence of the weak interactions between hydrogenated and fluorinated chains have on the flow in the absence of hydrogen bonding. This study was conducted at 343.15 K to speed up the molecular dynamics of the (HexOH + UFH) system, making the samplings faster.

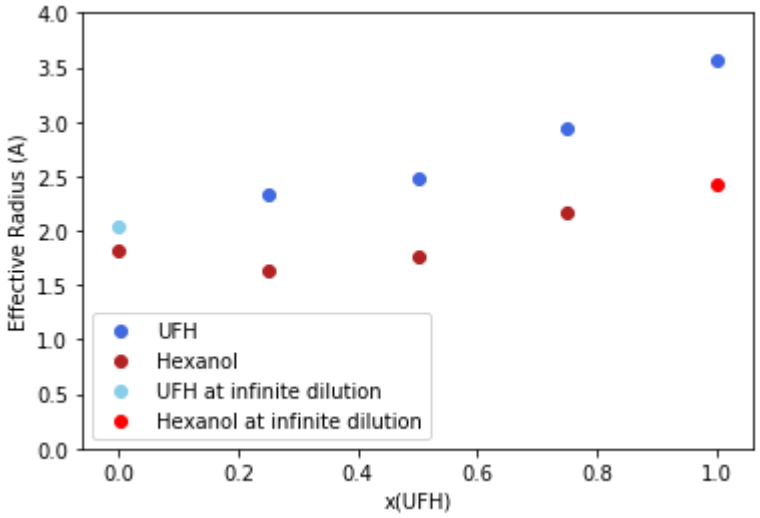

Figure 4.16: Effective radius of (HexOH + UFH) mixtures at 343.15 K with experimental viscosities

Although the uncertainty associated with the calculation of the effective radius is large (10%), the results suggests that when diluted in Hexanol, molecules of UFH tend to have a faster motion than when pure, as shown by the clear tendency of decreasing its effective radii when the concentration on Hexanol increases. Regarding Hexanol, the change of effective radius is much smaller. Nevertheless, the results seem to indicate that there is an initial slight decrease of the effective radius of Hexanol in the mixtures, increasing afterwards.

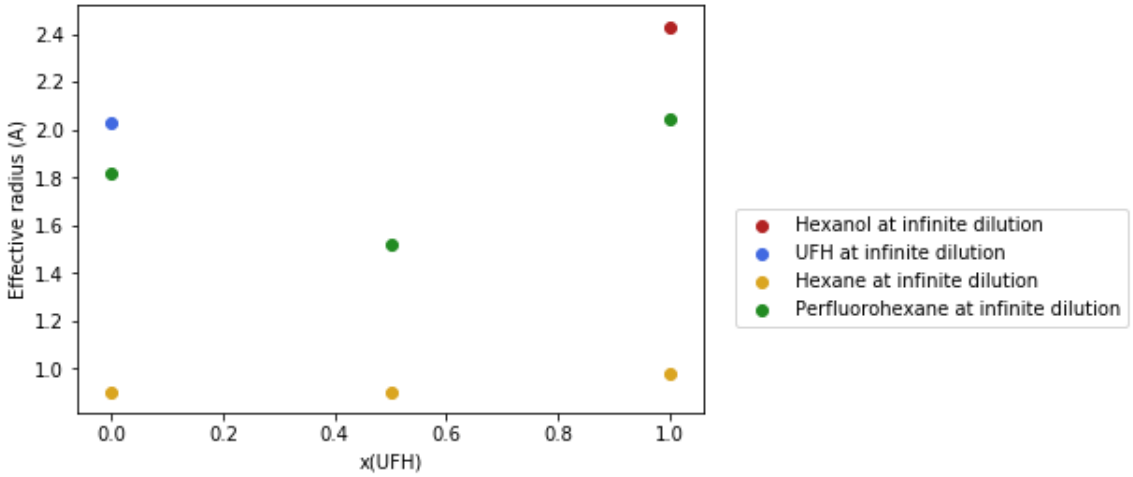

Figure 4.17: Effective radius of Hexane and Perfluorohexane at infinite dilution in a equimolar (HexOH + UFH) mixture and the pures plus, HexOH and UFH in infinite dilution at 343.15 K calculated with experimental viscosities

Firstly, this plot seems consistent concerning the molecules of Hexanol and UFH having higher effective radii than Hexane and Perfluorohexane. Since both alcohols hydroxyl group generate a nano structure consisting of a $O \cdots H$ network (this topic will be further explained in the next section), these molecules should have their movement constrained by such network. Since Hexane and Perflurohexane do not have hydroxyl groups, their movement should be easier than the alcohols, and consequently have a lower effective radii, as the plot suggests.

Secondly, the Perfluorohexane molecule decreases slightly its effective radius when infinitely diluted in Hexanol and even more significantly when in the equimolar mixture. This overall decrease could indicate that the weak dispersion interactions between hydrogenated and fluorinated chains can "help" the movement of the fluorinated chain.

The hexane effective radius seems to be much less affected by the composition of the solvent, this indicates that the mobility of hexane is very similar

in hexanol and in UFH, contrarily to perfluorohexane, whose mobility seems to increase with the content of hydrogenated solvent.

4.4 Liquid Structure

Intermolecular radial distribution functions (rdfs) provide a measure of the local structure in liquids. They were calculated from the simulation trajectories for the fluorinated chain of UFH and PFO and, the hydrogenated chain of Hexanol and Decanol, excluding the Hydrogens bonded to Carbon-1, and, the Oxygen and Hydroxyl group, not only for pure like interactions but also for cross-interactions. This rdfs are displayed in figures 4.18 and 4.21, for (HexOH + UFH) and, figures 4.19 and 4.25, for (DOH + PFO).

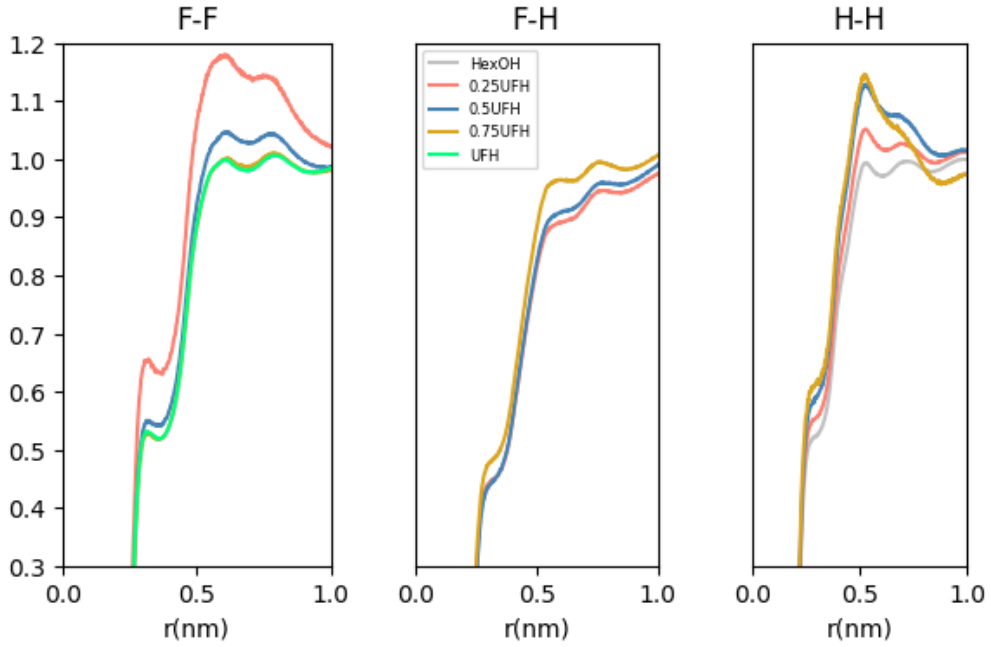

Figure 4.18: Intermolecular rdfs between the Hydrogen and Fluorine atoms (H or F) for (HexOH + UFH) mixtures at different compositions, from molecular dynamics simulations.

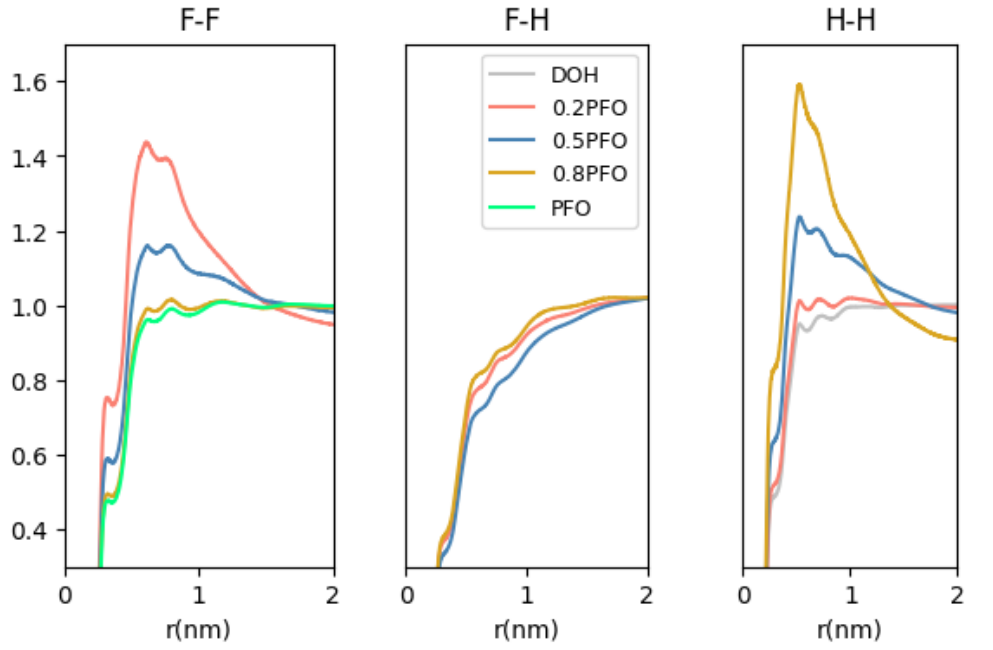

Figure 4.19: Intermolecular rdfs between the Hydrogen and Fluorine atoms (H or F) for (DOH + PFO) mixtures at different compositions, from molecular dynamics simulations.

Radial distribution functions generated for $H-H$ and $F-F$ group, increase notably with the increase in concentration of the second component. Also, the peaks of the highest rdfs are above one on both systems which reveals that nearby these fluorinated and hydrogenated chains there is a higher concentration of identical chains when compared with a random ensemble. This is a strong indication of segregation between hydrogenated and fluorinated segments and supports the hypothesis of the presence of clusters of fluorinated and hydrogenated chains in the mixture. It is important to keep in mind that this segregation is dictated by the weak cross interactions between alkyl and perfluoroalkyl chains. As expected, the $F-H$ rdf peak is below one which reveals that in these mixtures the meeting of these groups is less likely than on random ensembles. Figure 4.20a allows the visualization

of such segregation for the (HexOH + UFH) mixture and figure 4.20b for the (DOH + PFO) mixture.

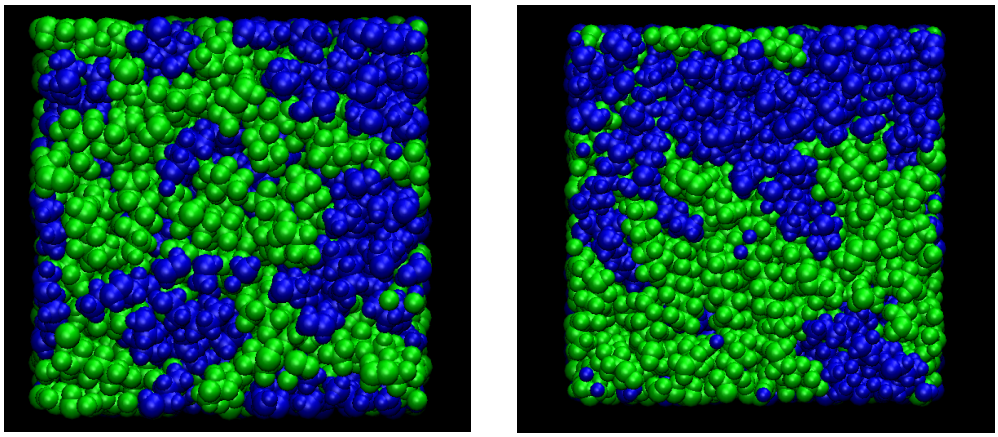

(a) HexOH + UFH (b) DOH + PFO

Figure 4.20: Snapshot of a MD simulation box consisting of an equimolar mixture. Alcohols (HexOH and DOH) are the blue chains and, fluorinated alcohols (UFH and PFO) are the green chains

Although mixing hydrogenated and fluorinated chains leads to nano-segregation of these molecules into domains, it is interesting to notice that despite this effect, the addition of the different alcohol also increases the variety of H-bonds. For (HexOH + UFH), some of the new established cross-hydrogen bonds are more frequent than those between identical molecules as revealed in figure 4.21 with the curve corresponding to hydrogen bonding between the Oxygen atom in HexOH (bearing the highest negative partial charge) and the Hydrogen atom (bearing the highest positive partial charge) in UFH being much more intense than the others. The reason beyond such strong bonding resides on the difference of the partial charges assigned to the interacting atoms. The presence of fluorine, with very high electronegativity, intensifies the ability of the OH group to form H-bonds by H donation and, consequently, establishing stronger H-bonds with the hydrogenated alcohols.

On the other hand, the H-bond between oxygen atom in UFH and the hydrogen atom in HexOH is least present in the mixture as the difference of the partial charges is the smallest. Steric effects can also explain these observations as the bulkier character of fluorine and the rigidity of fluorinated chains can make the interaction more sterically hindered.

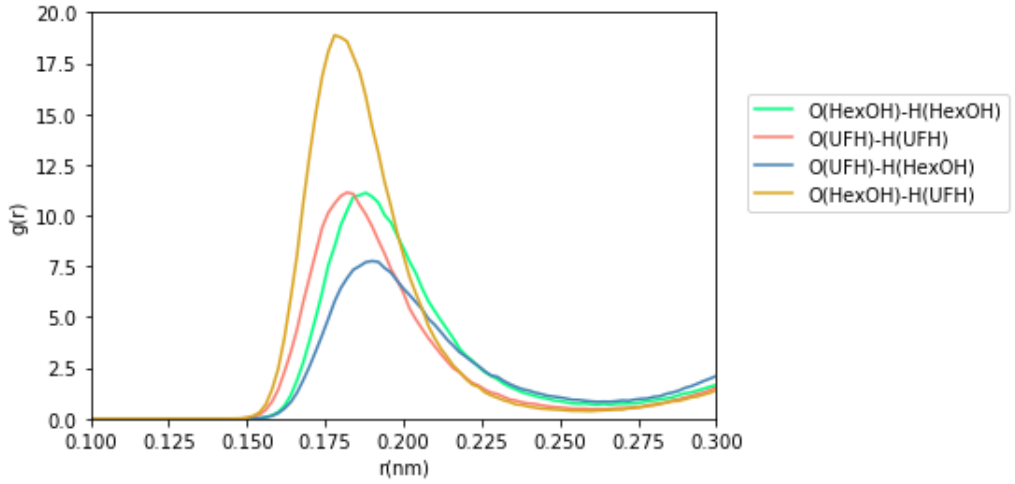

Figure 4.21: Intermolecular rdfs between the oxygen and hydroxyl hydrogen atoms for the (HexOH + UFH) at equimolar mixture.

The analysis of the rdfs indicates that similarly to what was previously seen by Morgado[17] for the (BuOH + HFB) system, mixtures of (HexOH + UFH) can be regarded as nanostructured. This nanostructure consists of a $O \cdots H$ network of hydrogen bonds formed between the hydroxyl headgroups, surrounded by the carbon chain tails, which, after being forced into approximating in the $O \cdots H$ network, segregate into hydrogenated and fluorinated domains.

To understand how this breakage and formation of H-Bonds may be responsible for the reported negative excess viscosities of both (HexOH + UFH) and (BuOH + HFB), similar to the (Decane + Hexanol) mixtures shown in figure 4.13, the distribution of hydrogen bonds between each type was calcu-

lated for the pures and equimolar mixture for (HexOH + UFH) and (BuOH + HFB), figure 4.26 and 4.23.

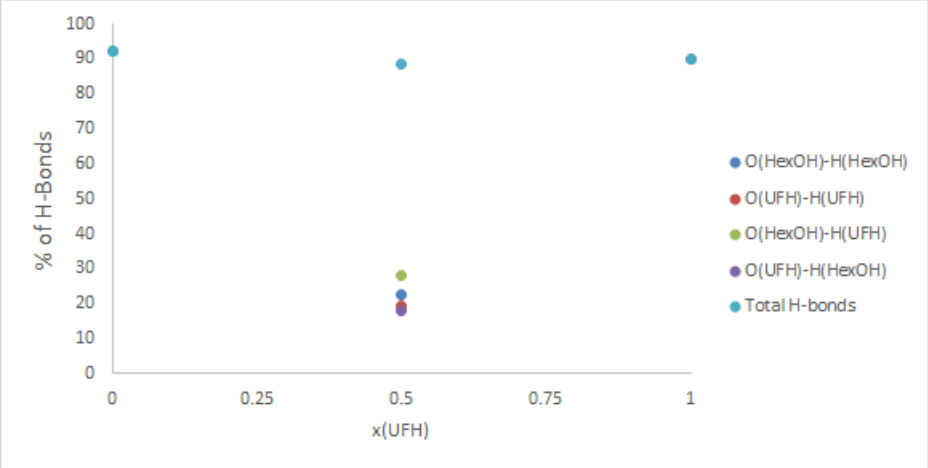

Figure 4.22: Distribution of H-Bonds in the (HexOH + UFH) mixture as function of composition, via computer simulation

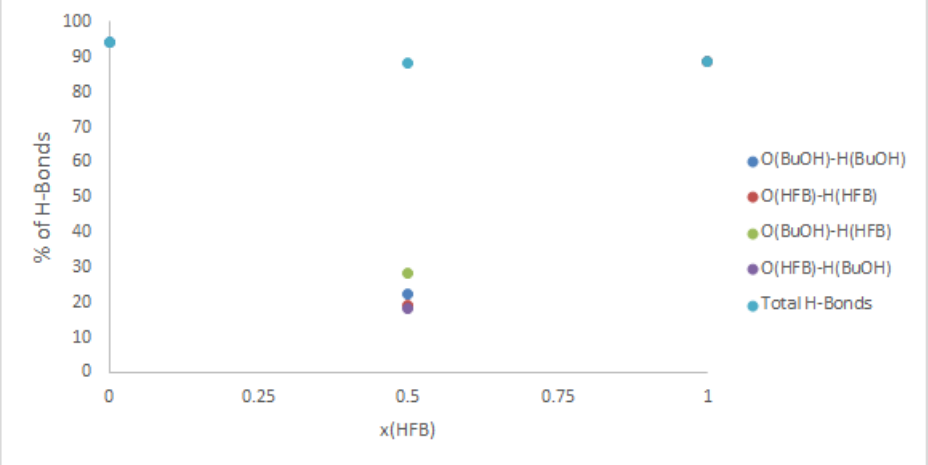

Figure 4.23: Distribution of H-Bonds in the (BuOH + HFB) mixture as function of composition, via computer simulation

In this scenario, 100% corresponds to the maximum number of hydrogen bonds, 2 for each molecule present in the system. The distribution for the (BuOH + HFB) is identical to that obtained by Morgado [17] with O(BuOH)-

H(HFB) being the more abundant, 28.5%, and, O(HFB)-H(BuOH) the least abundant, 18.4%, for the equimolar mixture. In turn, the distribution for the (HexOH + UFH) is very similar to the one obtained for (BuOH + HFB).

However, by mixing fluorotelomer alcohols and hydrogenated alcohols, the overall amount of hydrogenated bonds does not have a significant variation from the pures to the equimolar mixture, therefore it seems that the breakage and formation of hydrogen bonds is not responsible for the more fluid flow in the mixture in comparison to the pures.

Figure 4.24, is a molecular dynamics simulation snapshot obtained for an equimolar mixture of (HexOH + UFH) which illustrates such structure, for that purpose the size of the hydrogenated and fluorinated chains were reduced to highlight the hydroxyl groups network in the system.

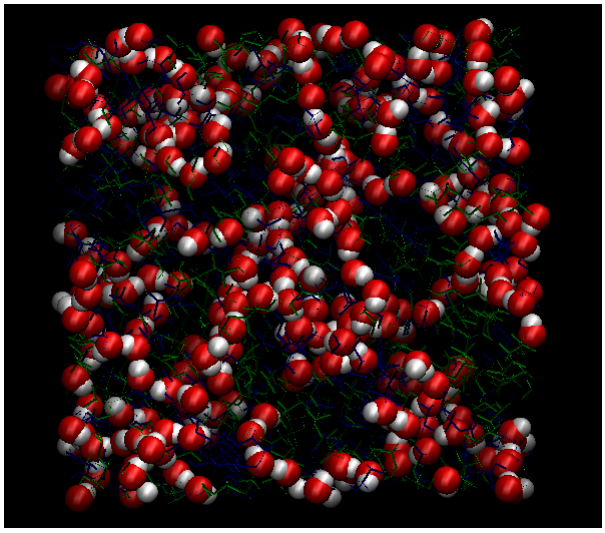

Figure 4.24: Snapshot of the $O \cdots H$ network in a MD simulation box consisting of an equimolar mixture of HexOH (blue chains) and UFH (green chains); coloured red are the Oxygen's of both molecules and white are the Hydrogen's

For the (DOH + PFO), the rdfs between the oxygen and hydroxyl hydrogen at 298.15 K were calculated for two compositions. Since this system

presents phase separation (solid + liquid) for compositions higher than 0.7, only mixtures with compositions bellow x(PFO)=0.6 were studied, namely 0.5 and 0.2.

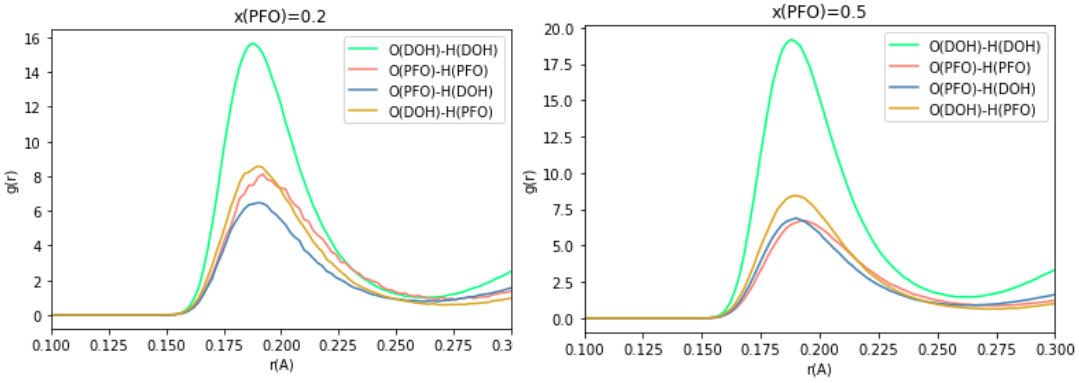

Figure 4.25: Intermolecular rdfs between the oxygen and hydroxyl hydrogen atoms for the (DOH + PFO) at two different compositions

An inversion in the order of rdfs of each type of hydrogen bonding for both compositions is observed. The rdfs show that in both compositions the $O(DOH) - H(DOH)$ H-bond is the predominant one, which did not occur in the (HexOH + UFH) and (BuOH + HFB)[17] systems. This may signify that, on contrary to the (HexOH + UFH) mixture, where the formed H-bonds have a more significant impact on the fluid organization, in this mixture, the weak dispersion interactions between the mutual phobic segments have a more important role in the structural arrangement of the fluid, which eventually leads to a higher level of segregation. Additionally, the distribution of H-Bonds was calculated as function of composition confirming the previous observations.

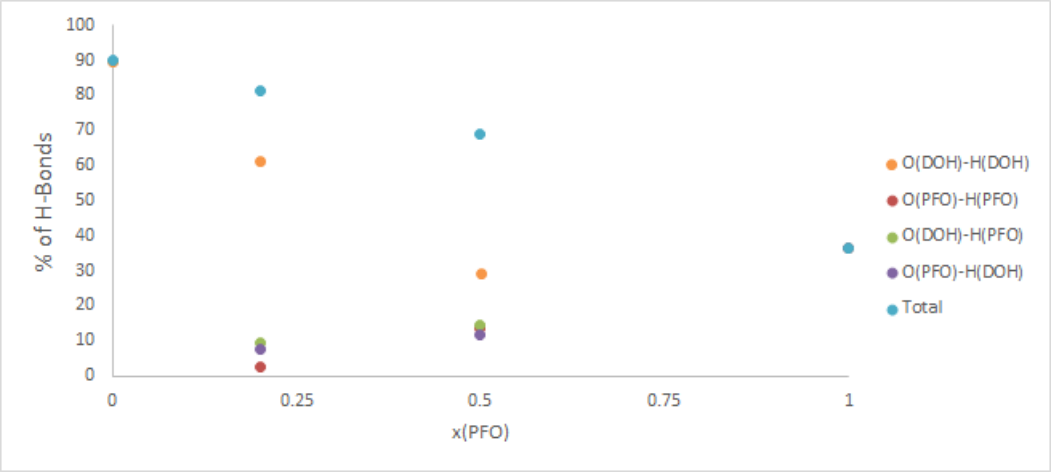

Figure 4.26: Distribution of H-Bonds in the (DOH + PFO) mixture as function of composition, via computer simulation

Chapter 5

Conclusions and Future Work

This computational study was able to successfully reproduce the densities and excess volumes and molar volumes of three different mixtures, namely, (BuOH + HFB), (HexOH + UFH) and (DOH + PFO). Also, the simulations and the calculation methodology used were able to reproduce experimental viscosities and excess viscosities for (BuOH + HFB) and (HexOH + UFH) mixtures.

The molecular dynamics simulations performed, seem to indicate that the large negative excess viscosities of mixtures of fluorinated and hydrogenated alcohols results from a combination of factors. The study of the diffusion coefficient and effective radii of fluorinated chains in these mixtures reveals an enhanced motion of fluorinated segments when in contact with hydrogenated alcohols due to the unfavourable dispersion forces between hydrogenated and fluorinated groups.

The results from the radial distribution functions show signs of existing mutual segregation between fluorinated and hydrogenated chains, generating domains of each kind, while simultaneously creating a $O \cdots HO$ network of Hydrogen bonding for (BuOH + HFB) and (HexOH + UFH). However, with the increase of the length of the fluorinated and hydrogenated segments, the $O \cdots HO$ network of Hydrogen bonding seems to loose importance in the determination of the fluid structure.

Regarding the experimental measurements, the comparison of the re-

ported viscosities for 2,2,3,3,4,4,5,5,6,6,7,7,7-tridecafluoroheptan-1-ol with other fluorotelomer alcohols, present in literature, show a good agreement.

From a fundamental point of view it would be interesting, in future works, to understand the possible and preferential arrangements of the clusters of hydrogenated and fluorinated chains. Also, the subtlety of identifying and defining domains requires a further development of the available tools capable of analysing the trajectory of a molecular dynamics simulation. Moreover, the effects that an increase in either the fluorinated or the hydrogenated chain has on the excess properties of this mixtures would be an important step to separate the role each of chains has on the mentioned properties.

Finally, the study of the drastic changes in the structural arrangement of the (DOH + PFO) mixture would allow to further understand the impact the weak dispersion forces between fluorinated and hydrogenated segments have on the thermodynamic properties of alcohol and fluorotelomer alcohol mixtures. This mixture seems to be a tipping point between the influence of the mutual phobic segments and the polar alcoholic group in the determination of the liquid structure.

Bibliography

[1] M. Abraham, E. Lindahl, B. Hess, and GROMACS Development Team. GROMACS User Manual version 2018, 2018.

[2] C. S. Adorf, P. M. Dodd, V. Ramasubramani, and S. C. Glotzer. Simple data and workflow management with the signac framework. *Computational Materials Science*, 146:220–229, 2018.

[3] M. P. Allen and D. J. Tildesley. *Computer Simulation of Liquids*. Oxford Science Press, second edi edition, 2017.

[4] R. Chitra and P. E. Smith. A comparison of the properties of 2,2,2-trifluoroethanol and 2,2,2-trifluoroethanol/water mixtures using different force fields. *Journal of Chemical Physics*, 115(12):5521–5530, 2001.

[5] M. A. Costa. Property Data and Phase Equilibria for the Design of Chemical Processes involving Carbon Dioxide, 2017.

[6] M. G. Freire, A. G. Ferreira, I. M. Fonseca, I. M. Marrucho, and J. A. Coutinho. Viscosities of liquid fluorocompounds. *Journal of Chemical and Engineering Data*, 53(2):538–542, 2008.

[7] M. A. González. Force fields and molecular dynamics simulations. *Collection SFN*, 12:169–200, 2011.

[8] M. D. Hanwell, D. E. Curtis, D. C. Lonie, T. Vandermeerschd, E. Zurek, and G. R. Hutchison. Avogadro: An advanced semantic chemical editor, visualization, and analysis platform. *Journal of Cheminformatics*, 4(8), 2012.

[9] B. Hess, H. Bekker, H. J. Berendsen, and J. G. Fraaije. LINCS: A Linear Constraint Solver for molecular simulations. *Journal of Computational Chemistry*, 18(12):1463–1472, 1997.

[10] W. L. Jorgensen, D. S. Maxwell, and J. Tirado-Rives. Development and testing of the OPLS all-atom force field on conformational energetics and properties of organic liquids. *Journal of the American Chemical Society*, 118(45):11225–11236, 1996.

[11] C. Klein, J. Sallai, T. J. Jones, C. R. Iacovella, C. McCabe, and P. T. Cummings. A Hierarchical, Component Based Approach to Screening Properties of Soft Matter. *Foundations of Molecular Modeling and Simulation*, pages 79–92, 2016.

[12] D. M. Lemal. Perspective on Fluorocarbon Chemistry. *Journal of Organic Chemistry*, 69(1):1–11, 2004.

[13] L. Lepori, E. Matteoli, A. Spanedda, C. Duce, and M. R. Tiné. Volume changes on mixing perfluoroalkanes with alkanes or ethers at 298.15 K. *Fluid Phase Equilibria*, 201(1):119–134, 2002.

[14] L. F. Martins, L. A. Pereira, G. M. Silva, J. R. Ascenso, P. Morgado, J. P. Ramalho, and E. J. Filipe. Fluorinated surfactants in solution: Diffusion coefficients of fluorinated alcohols in water. *Fluid Phase Equilibria*, 407:322–333, 2015.

[15] P. D. Mobley, A. V. Rayer, J. Tanthana, T. R. Gohndrone, M. Soukri, L. J. Coleman, and M. Lail. CO2Capture Using Fluorinated Hydrophobic Solvents. *Industrial and Engineering Chemistry Research*, 56(41):11958–11966, 2017.

[16] P. Morgado, J. Black, J. B. Lewis, C. R. Iacovella, C. McCabe, L. F. Martins, and E. J. Filipe. Viscosity of liquid systems involving hydrogenated and fluorinated substances: Liquid mixtures of (hexane+perfluorohexane). *Fluid Phase Equilibria*, 358:161–165, 2013.

[17] P. Morgado, A. R. Garcia, L. M. Ilharco, J. Marcos, M. Anastácio, L. F. G. Martins, and E. J. M. Filipe. Liquid Mixtures Involving Hydrogenated and Fluorinated Alcohols: Thermodynamics, Spectroscopy, and Simulation. *The Journal of Physical Chemistry B*, page acs.jpcb.6b04297, 2016.

[18] P. Morgado, C. M. Laginhas, J. B. Lewis, C. McCabe, L. F. Martins, and E. J. Filipe. Viscosity of liquid perfluoroalkanes and perfluoroalkylalkane surfactants. *Journal of Physical Chemistry B*, 115(29):9130–9139, 2011.

[19] O. A. Moultos, I. N. Tsimpanogiannis, A. Z. Panagiotopoulos, J. P. M. Trusler, and I. G. Economou. Atomistic Molecular Dynamics Simulations of Carbon Dioxide Diffusivity in n-Hexane, n -Decane, n -Hexadecane, Cyclohexane, and Squalane. *The Journal of Physical Chemistry B*, 120(50):12890–12900, 2016.

[20] S. Nosé. A molecular dynamics method for simulations in the canonical ensemble. *Molecular Physics*, 52(2):255–268, 1984.

[21] T. Okazoe. Overview on the history of organofluorine chemistry from the viewpoint of material industry. *Proceedings of the Japan Academy, Series B*, 85(8):276–289, 2009.

[22] A. A. Pádua. Torsion energy profiles and force fields derived from Ab initio calculations for simulations of hydrocarbon-fluorocarbon di-

blocks and perfluoroalkylbromides. *Journal of Physical Chemistry A*, 106(43):10116–10123, 2002.

[23] M. Parrinello and A. Rahman. Polymorphic transitions in single crystals: A new molecular dynamics method. *Journal of Applied Physics*, 52(12):7182–7190, 1981.

[24] L. A. Pereira, L. F. Martins, J. R. Ascenso, P. Morgado, J. P. Ramalho, and E. J. Filipe. Diffusion coefficients of fluorinated surfactants in water: Experimental results and prediction by computer simulation. *Journal of Chemical and Engineering Data*, 59(10):3151–3159, 2014.

[25] K. Pluhackova, H. Morhenn, L. Lautner, W. Lohstroh, K. S. Nemkovski, T. Unruh, and R. A. Böckmann. Extension of the LOPLS-AA Force Field for Alcohols, Esters, and Monoolein Bilayers and its Validation by Neutron Scattering Experiments. *Journal of Physical Chemistry B*, 119(49):15287–15299, 2015.

[26] R. Renner. The long and the short of perfluorinated replacements. *Environmental Science and Technology*, 40(1):12–13, 2006.

[27] D. V. Spoel, E. Lindahl, B. Hess, and G. Groenhof. GROMACS: Fast, Flexible, and Free. *Journal of Computational Chemistry*, 26(16):1701–18, 2005.

[28] E. K. Watkins and W. L. Jorgensen. Perfluoroalkanes: Conformational Analysis and Liquid-State Properties from ab Initio and Monte Carlo Calculations. *Journal of Physical Chemistry A*, 105(16):4118–4125, 2001.

[29] Y. Zhang, A. Otani, and E. J. Maginn. Reliable Viscosity Calculation from Equilibrium Molecular Dynamics Simulations: A Time De-

composition Method. *Journal of Chemical Theory and Computation*, 11(8):3537–3546, 2015.

Appendix A

Experimental measurements

Table A.1: Experimental viscosities as function of temperature of 2, 2, 3, 3, 4, 4, 5, 5, 6, 6, 7, 7, 7-tridecafluoroheptan-1-ol

T(K)	η **(mPa.s)**
283.15	46.161
288.15	33.634
293.15	24.983
298.15	18.892
303.15	14.532
308.15	11.362
313.15	9.0192
318.15	7.2633
323.15	5.9283
328.15	4.8997
333.15	4.0967
338.15	3.4617
343.15	2.9538
348.15	2.5440
353.15	2.2088

Appendix B

Simulated Viscosities and Excess Viscosities

Table B.1: Simulated viscosities and excess viscosities of (Butanol + HFB) at 293.15 K and 313.15 K

	T=293.15K			T=313.15K		
x1(HFB)	η (cP)	SD	100 $\Delta\eta/\eta$	η (cP)	SD	100 $\Delta\eta/\eta$
0	2.64	1.04	0.0	1.48	0.61	0.0
0.25	2.71	1.11	-26.8	1.58	0.61	-16.3
0.5	3.38	1.48	-28.9	1.79	0.78	-21.8
0.75	4.17	1.53	-28.2	2.42	0.83	-10.5
1	6.87	2.78	0.0	3.11	1.26	0.0

Table B.2: Simulated viscosities and excess viscosities of (Hexanol + UFH) at 293.15 K and 313.15K

	T=293.15K			T=313.15K		
x1(UFH)	η (cP)	SD	100 $\Delta\eta/\eta$	η (cP)	SD	100 $\Delta\eta/\eta$
0	4.36	1.74	0.0	2.34	0.89	0
0.25	4.52	1.79	-46.5	2.54	1.02	-32.6
0.5	7.74	3.10	-38.4	3.64	1.33	-29.8
0.75	11.71	4.33	-29.7	5.02	2.09	-24.1
1	20.77	8.90	0.0	8.04	3.74	0.0

Table B.3: Simulated viscosities and excess viscosities of (Hexanol + UFH) at 343.15 K

	T=343.15K		
x1 (UFH)	η (cP)	SD	100 $\Delta\eta/\eta$
0	1.20	0.44	0.0
0.25	1.33	0.54	-10.0
0.5	1.44	0.58	-13.2
0.75	1.98	0.80	-11.2
1	2.92	1.13	0.0

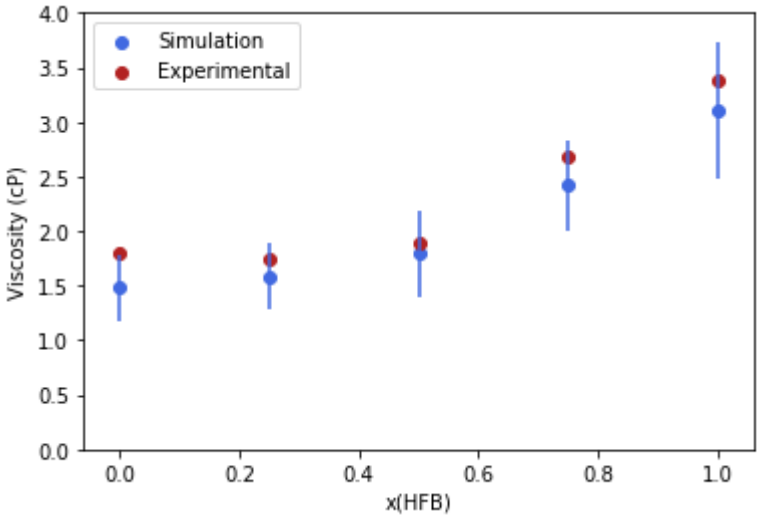

Figure B.1: Experimental and simulated viscosities of (Butanol + HFB) at 313.15 K

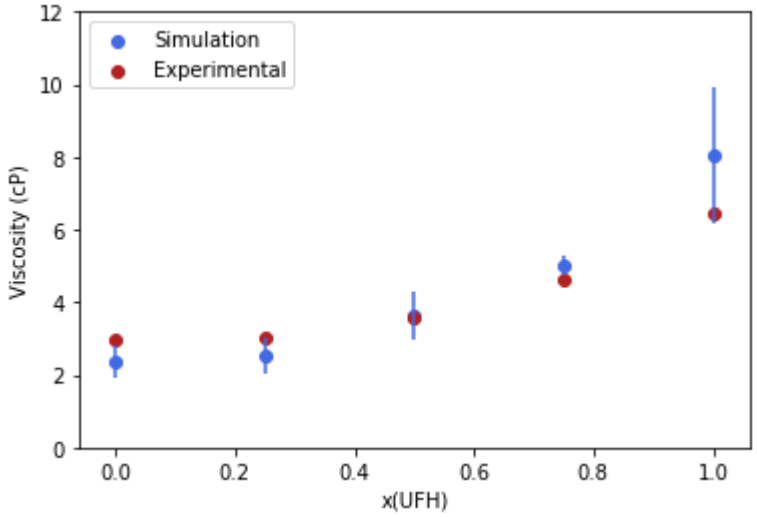

Figure B.2: Experimental and simulated viscosities of (Hexanol + UFH) at 313.15 K

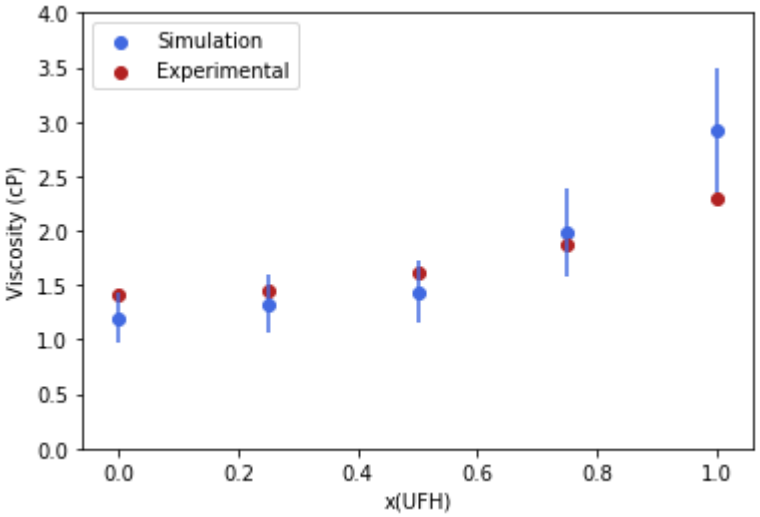

Figure B.3: Experimental and simulated viscosities of (Hexanol + UFH) at 343.15 K

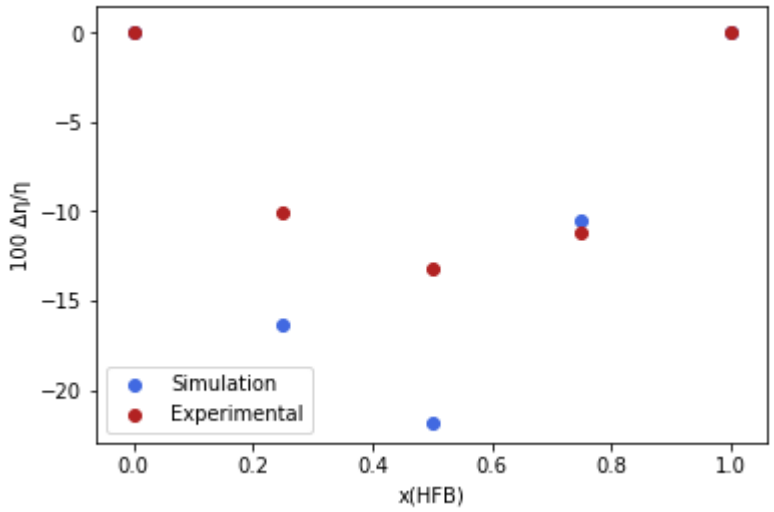

Figure B.4: Experimental and simulated excess viscosities for (Butanol + HFB) at 313.15 K

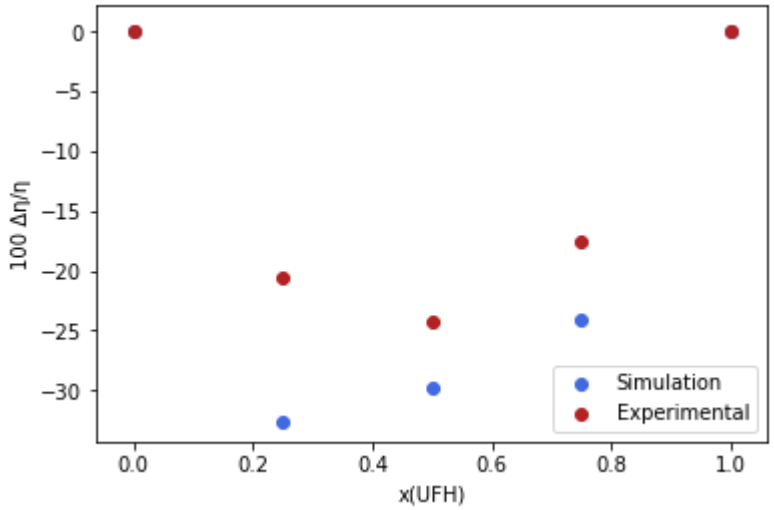

Figure B.5: Experimental and simulated excess viscosities for (Hexanol + UFH) at 313.15 K

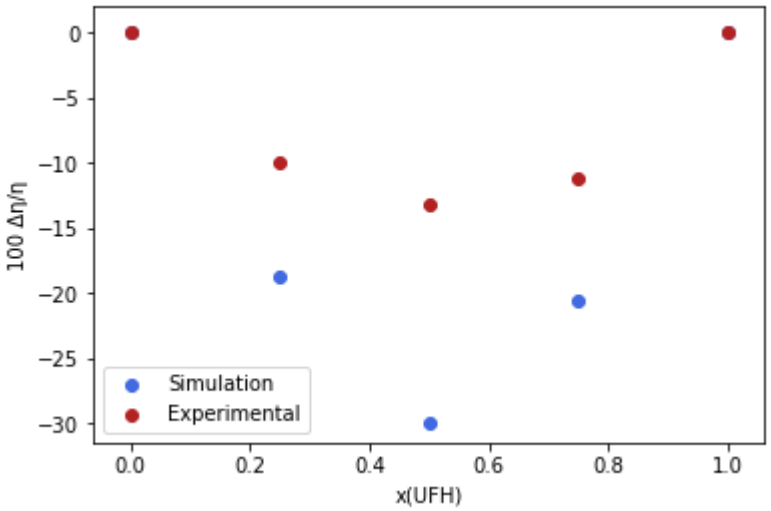

Figure B.6: Experimental and simulated excess viscosities for (Hexanol + UFH) at 343.15 K

Appendix C

Simulated Diffusion Coefficients

Table C.1: Simulated diffusion coefficients of (Hexanol+UFH) at 293.15 K and 343.15K

	T=293.15 K				T=343.15 K			
	UFH		HexOH		UFH		HexOH	
x1(UFH)	D (cm2/s)	Deviation	D (cm2/s)	SD	D (cm2/s)	SD	D (cm2/s)	SD
0			1.89E-06	2.3E-07			9.85E-06	1.40E-06
0.25	1.49E-06	1.0E-07	1.70E-06	1.6E-07	7.6E-06	5.5E-07	1.07E-05	7.8E-07
0.5	1.09E-06	1.3E-07	1.37E-06	1.7E-07	6.3E-06	7.5E-07	8.88E-06	8.7E-07
0.75	6.01E-07	1.2E-07	8.20E-07	2.2E-07	4.6E-06	5.1E-07	6.23E-06	9.1E-07
1	4.11E-07	4E-08			3.1E-06	8.5E-07		

Table C.2: Simulated diffusion coefficients of (Butanol+HFB) at 293.15 K

	T=293.15 K			
	HFB		BuOH	
x1(HFB)	D (cm2/s)	SD	D (cm2/s)	SD
0			3.69E-06	5.2E-07
0.25	3.05E-06	4.7E-07	3.93E-06	3.8E-07
0.5	2.65E-06	3.6E-07	3.27E-06	3.4E-07
0.75	2.01E-06	1.8E-07	2.70E-06	2.7E-07
1	1.61E-06	1.8E-07		